Geophysics Open-File Report 50
Geoscience Department and
Geophysical Research Center
New Mexico Tech, Socorro, NM 87801

CHARACTERISTICS AND POSSIBLE CAUSE OF AN EARTHQUAKE SWARM IN THE CENTRAL RIO GRANDE RIFT 28 KM NORTH OF SOCORRO, NEW MEXICO: FEBRUARY AND MARCH, 1983

by

Stephen Jarpe

Submitted in partial fulfillment
of the requirement for
Geophysics 590
and the
Master of Science Degree Program

at

NEW MEXICO INSTITUTE OF MINING AND TECHNOLOGY

Socorro, New Mexico

May, 1984

ABSTRACT

Between February 25 and March 16, 1983, an earthquake swarm consisting of approximately 300 recorded shocks (100 above magnitude 0.0) occurred 28 km north of Socorro in the central Rio Grande rift. Included within the swarm was a magnitude 4.0 earthquake, the largest in the Socorro area since 1961. A temporary seismograph array surrounding the swarm area, in addition to the eight permanent stations in the Socorro network, allowed precise locations of 28 of the larger shocks occurring after the main shock. For these well constrained solutions, the average 2 standard deviation errors in the depth of focus and in the epicentral location were 0.6 km and 0.4 km, respectively.

The depths of focus for the swarm earthquakes ranged from 4.8 to 7.8 km, with a mean of 6.5 km. These depths of focus are significantly less than for earthquake swarms 30 km to the south. No systematic migration of hypocenters with time was observed. The hypocenters define a planar volume that trends N25°E and dips 50 degrees to the east. This orientation is in agreement with one of the nodal planes of a normal fault plane solution obtained for the main shock from an analysis of first motions. This suggests that the aftershocks occurred mostly on the fault plane of the main shock. The roughly N-S strike and 50 degree dip of the fault plane also agrees with the orientations of recent (< 4 m.y. old) surface normal faults in the Rio Grande rift.

The first motion distributions of thirteen aftershocks cannot be explained by the standard double couple without moment (DCWM) model of faulting. These unusual first motion distributions may be explained by a combination of two or more possible mechanisms, including the DCWM. Other possible mechanisms are 1) the linear vector dipole (LVD), which results from the formation of a tensile crack, 2) an explosive source, which could result from the contact of magma with water, and 3) the compensated linear vector dipole (CLVD), which results from the formation of a tensile crack accompanied by an influx of fluid into the crack.

The swarm is located at the center of a region of surface uplift defined by level-line data, and above an extensive (> 1700 km^2) layer of magma at a depth of about 19 km. A possible cause for the swarm is upward migration of magma from the mid-crustal magma body along pre-existing fault zones.

TABLE OF CONTENTS

ACKNOWLEDGEMENTS

I would like to thank first and foremost Dr. Allan Sanford, who provided invaluable inspiration and guidance. Thanks are also due to Jon Ake, for many hours of helpful discussion, and to Larry Jaksha, for providing much of the data and for his helpful comments. Help with the data analysis was provided by undergraduate assistants Scott Phelps and Shirley Wade.

The New Mexico Tech Geophysical Research Center funded part of the project, and the New Mexico Tech Computer Center provided computer support.

INTRODUCTION

Between February 25 and March 16, 1983, a swarm of earthquakes consisting of over 300 recorded events (100 above magnitude 0.0) occurred in the central Rio Grande rift near Socorro. The swarm included a magnitude 4.0 earthquake, the largest in the central rift since 1961. The swarm was located about two kilometers east of the rest stop on Interstate-25, which is 28 kilometers north of Socorro between the San Acacia and the La Joya state game refuge exits.

The purpose of this study was to determine the general characteristics of the swarm, to locate as accurately as possible the larger earthquakes in the swarm, to determine the focal mechanisms of the earthquakes, and ultimately to get a better understanding of the processes that led to the occurrence of the swarm.

The earthquake swarm that is the topic of this study will be called the Rest Stop Swarm (RSS), after the nearest demographic feature.

Many previous articles describe the general characteristics of the Rio Grande rift. Two of the most comprehensive sources are Rio Grande Rift: Tectonics and Magmatism, edited by Riecker (1979), and the Guidebook to the Rio Grande Rift in New Mexico and Colorado, compiled by Hawley (1978). The major geographic and physiographic features of the Socorro area are outlined in Figure 1.

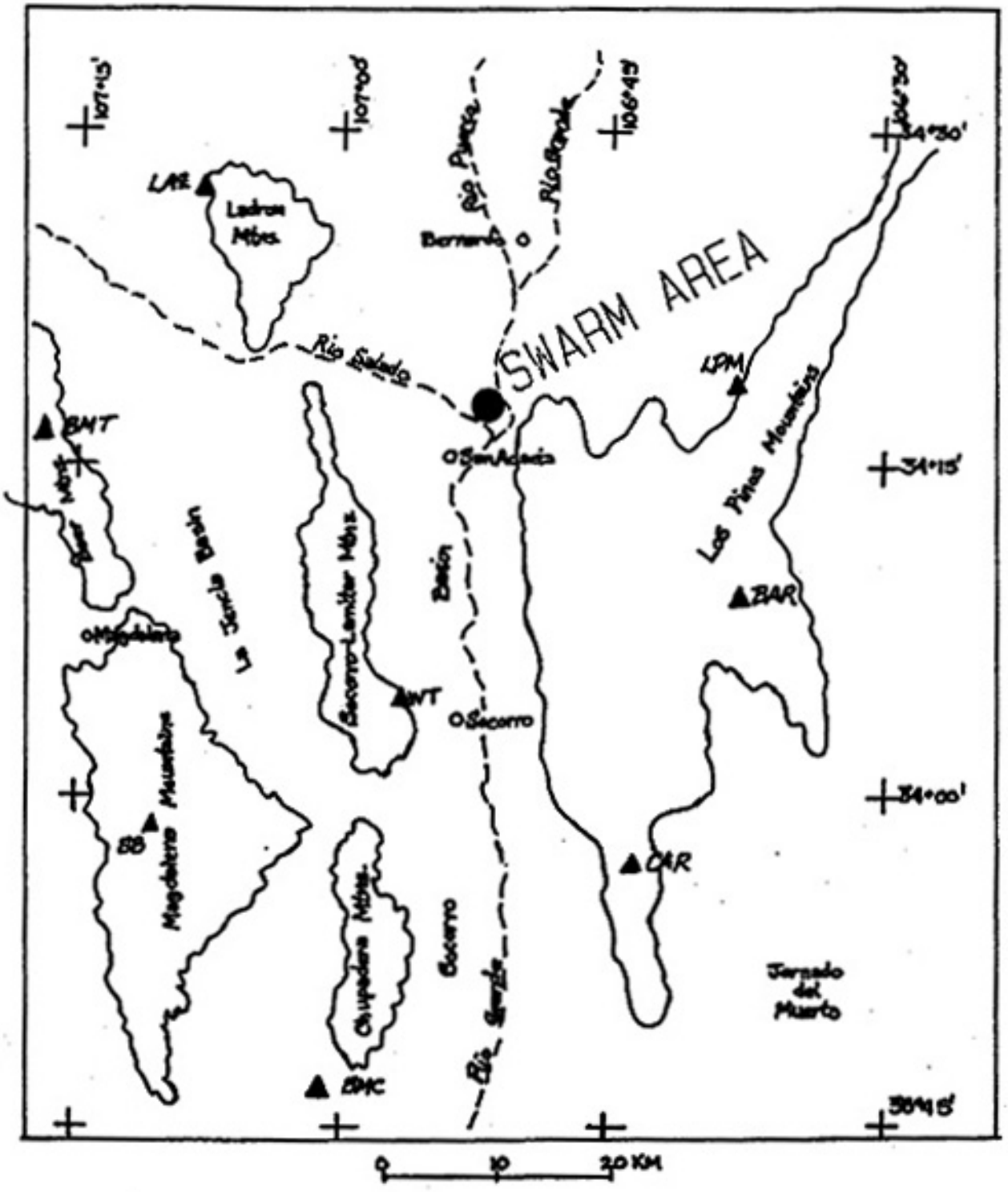

Figure 1. Major geographic features and physiographic provinces of the Socorro area. The dark triangles represent the USGS-NMT station array in March, 1983.

TECTONIC, GEOLOGICAL, AND GEOPHYSICAL SETTING

A possible explanation for the occurrence of earthquake swarms in the Socorro area is that magma is being injected into the upper crust from mid-crustal depths. For a more detailed discussion, see Sanford (1983), and Sanford and others (1983). Certain characteristics of the central rift that support magma migration as the cause of the Rest Stop Swarm will be outlined here.

Mid-Crustal Magma Body

The detection of magma in the mid-to-upper crust of the central Rio Grande rift forms a large part of the research at New Mexico Tech. The current status of this research is summarized by Sanford (1983). The position of the RSS is approximately over the center of an extensive sill-like mid-crustal magma body at about 19 km depth. The properties of the magma body have been studied extensively, and are summarized by Sanford (1983). The proposed outline of the magma body is shown in Figure 2.

Surface Uplift

There appears to be a zone of surface uplift associated with the mid-crustal magma body, possibly a result of the inflation of the body. A recent paper by Larsen and Reilinger (1983) updates the status of measurements of crustal deformation in the central Rio Grande rift (Reilinger and others, 1980). Their findings, based on

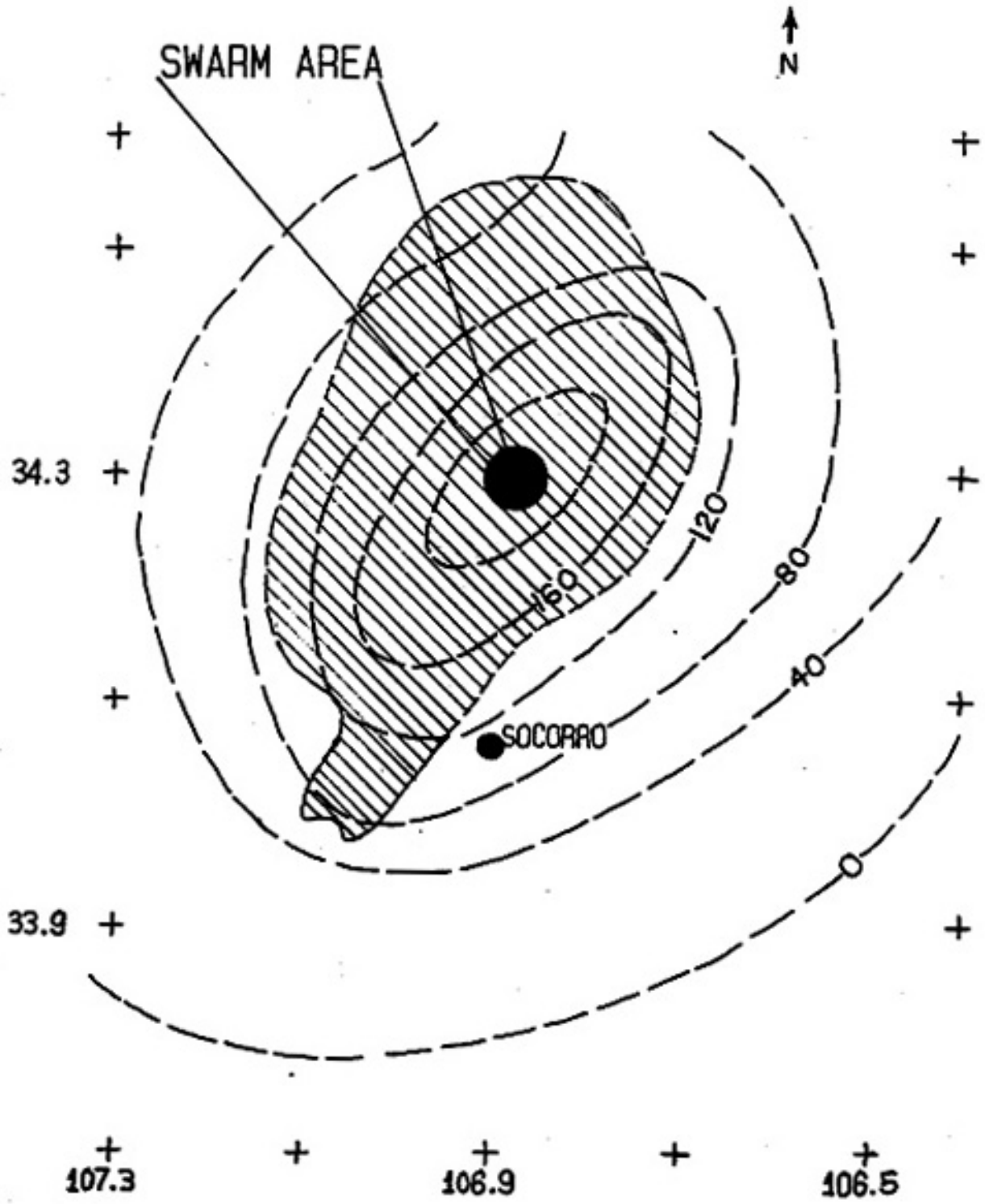

Figure 2. Location of the Rest Stop Swarm with the outline of the mid-crustal magma body (hatched) (from Sanford, 1983b), and contours of surface uplift in millimeters for the period 1910-1950 (from Reilinger and others, 1980).

level-line data, indicate a zone of crustal uplift between Socorro and Belen, with the maximum uplift at approximately the location of the RSS. Figure 2 shows their contours of surface uplift for the 40-year period 1910 to 1950 along with the location of the RSS. Maximum uplift for this period was 200 mm, which yields an average uplift rate of 5 mm/year. Between 1951 and 1980, the maximum uplift was 53 +/- 15 mm, which yields an uplift rate of 1.8 +/- 0.5 mm/yr.

Upper Crustal Magma

Several previous studies have attempted to identify magma in the upper crust of the central Rio Grande rift. The most convincing of these, by Ward (1980), used an inversion process to determine P-wave velocities of different blocks of crust in the Socorro area using micro-earthquake travel times. Inversion studies have the advantage that both errors in and the uniqueness of the final model parameters are determined along with the parameters. Ward used two different models; a 36 block model in which the blocks (0.1 deg x 0.1 deg) extended from the surface to about 10 km depth, and a 48 block model that had 36 blocks extending from the surface to 4 km depth, and 12 more blocks that extended from 4 km to about 10 km (see Ward and others, 1981). For the 36 block model, the block containing the RSS had a uniquely low velocity compared to all adjacent blocks at the two standard deviation (s.d.) level. For the 48 block model, neither the upper nor the

lower block containing the RSS had a uniquely determined low velocity with respect to adjacent blocks. Figures 3 and 4 show the final 36 block model and the final 48 block model along with the location of the RSS. A significantly lower velocity for one of the blocks of crust could indicate the presence of magma in that block.

Seismicity

The Socorro area is recognized as the most seismically active area of the Rio Grande rift (Sanford and others, 1983). Most of the earthquakes occur in swarms, and most of the larger events are associated with swarms. Since 1960, the general area of the RSS has been the most active in terms of numbers of large shocks (Sanford and others, 1983).

The seismicity of the Socorro area was monitored by the USGS-Albuquerque Seismological Laboratory between January, 1976, and November, 1981. During this 71 month period, the seismic network was in operation for 66 months. Figure 5 shows the earthquake epicenters located by the network for the 71 month period, along with the locations of the stations in the network (from L. Jaksha, in preparation). The estimated errors in the epicenters (about 2 km) do not permit any observations about the activity in the immediate area of the Rest Stop Swarm, but Figure 5 does show that the swarm area is about at the center of a well-defined zone of high seismicity with an areal extent of about 5000 km^2.

With the deployment of the USGS-NMIMT Socorro area

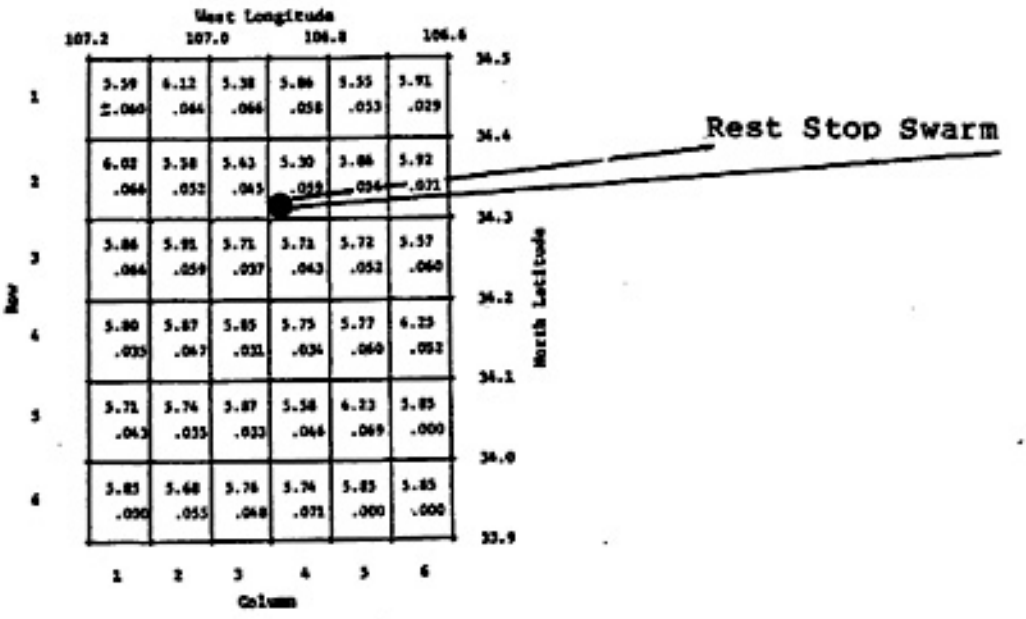

Figure 3. Ward's (1980) thirty-six block velocity model obtained from the damped least-squares inversion of travel-time data. The velocities and their uncertainties (one s.d.) are given.

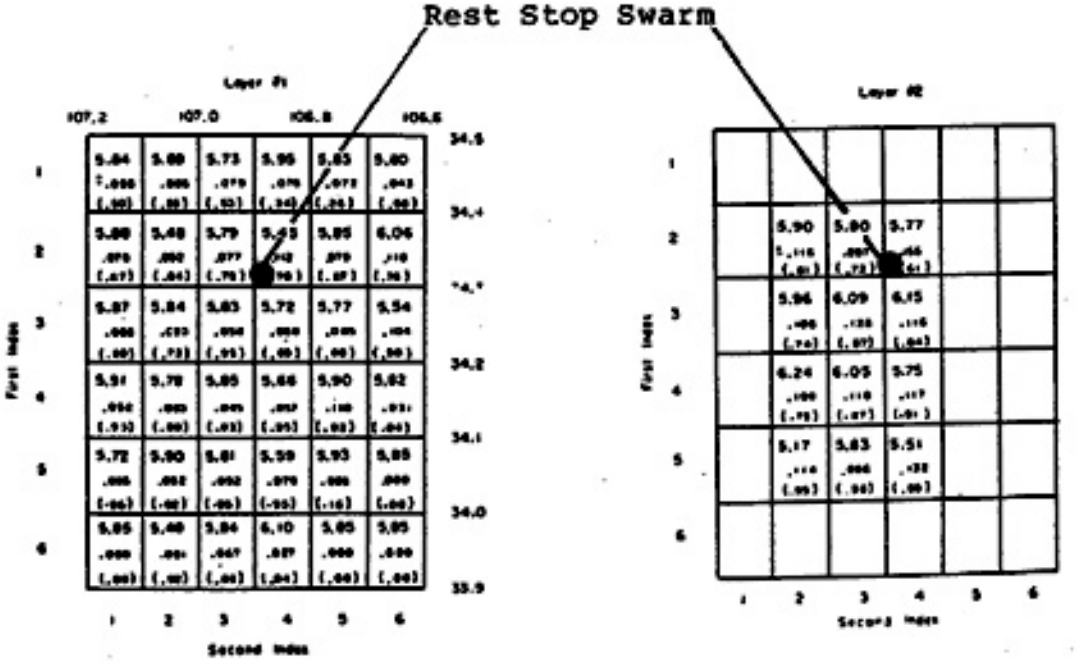

Figure 4. Ward's (1980) forty-eight block velocity model calculated using a generalized least-squares inversion of travel-times. Also given along with the velocities in km/sec are their one s.d. uncertainties and the diagonal elements of the corresponding resolving kernels. Also see Ward and others (1981).

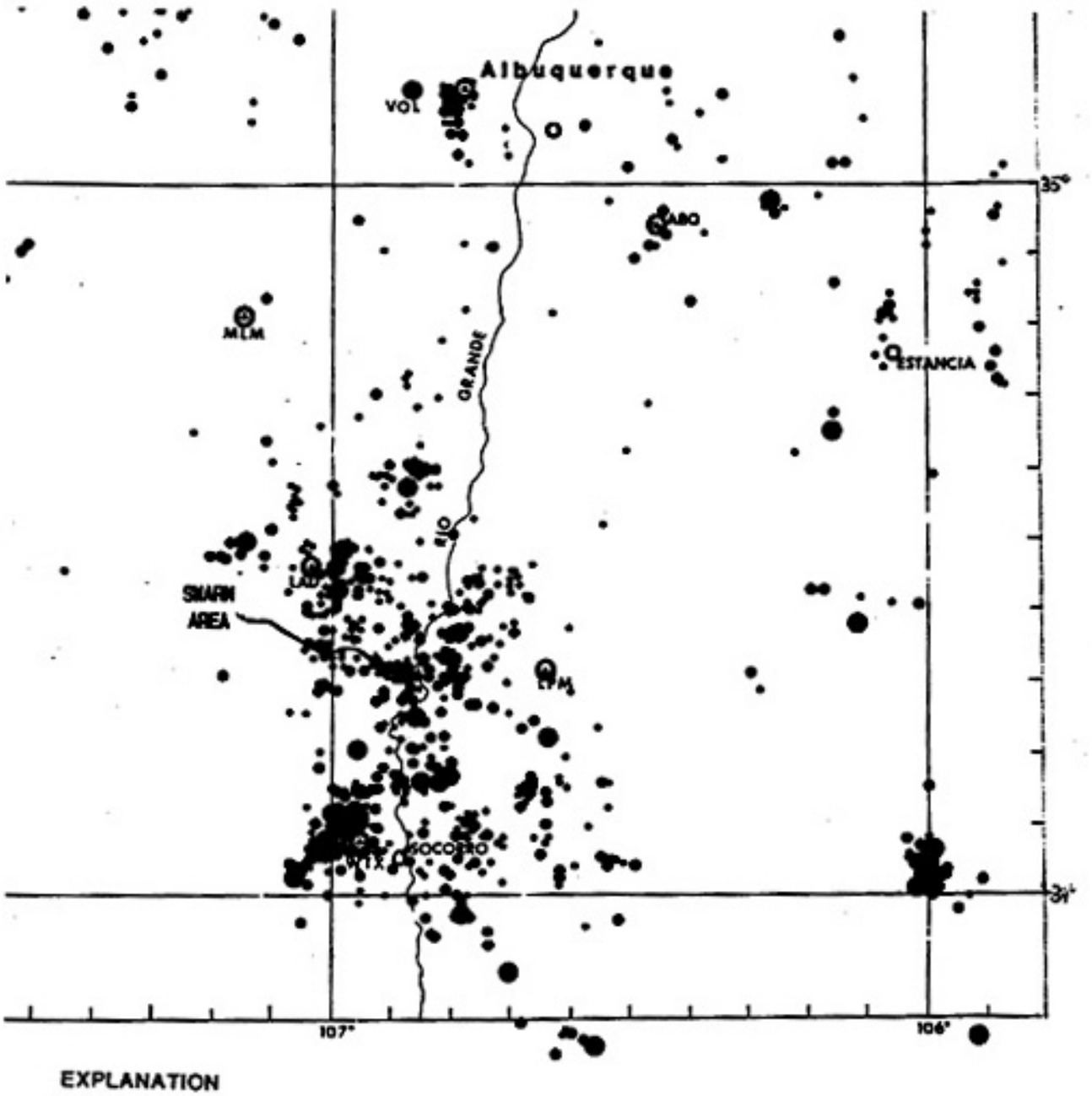

Figure 5. Earthquake activity in the central Rio Grande rift for 66 months of the 71 month period between January, 1976 and November, 1981. The estimated errors in the epicenters are approximately 2 km. The earthquakes were located by the USGS-ASL using the station array denoted by the triangular symbols (from L. Jaksha, in preparation).

seismic array in early 1982, more accurate locations of earthquakes in the RSS area became available. Figure 6 shows the earthquake activity between January 1, 1982 and February 24, 1983 (beginning of RSS) in an area 0.2 degrees of latitude by 0.3 degrees of longitude centered on the RSS area. The estimated (2 s.d.) errors in the epicenters are about 1 km. Although there is considerable activity 5 km to the east of the RSS, there were no detectable earthquakes within the area involving the RSS in the fourteen months preceding the onset of the swarm.

Recent Volcanism

Numerous volcanics less than 3 m.y. old have been identified in the Rio Grande rift between Santa Fe and Truth or Consequences by Bachman and Mehnert (1978). The youngest of these volcanic rocks are the basalt flows at the Albuquerque volcanoes 130 km north of Socorro, some of which have been dated as young as 0.19 +/- 0.04 m.y. The presence of young basalt flows in the central Rio Grande rift suggests that surface magmatic activity has occurred quite recently, although the amount of activity at any one time appears to have been small.

Recent Faulting

Numerous Pliocene and younger normal faults have been mapped in the central rift. They generally trend in a N-S direction, in agreement with E-W extension of the rift. Pliocene and younger faults in the RSS area as mapped by Machette and McGimsey (1983) are shown on Figure 7.

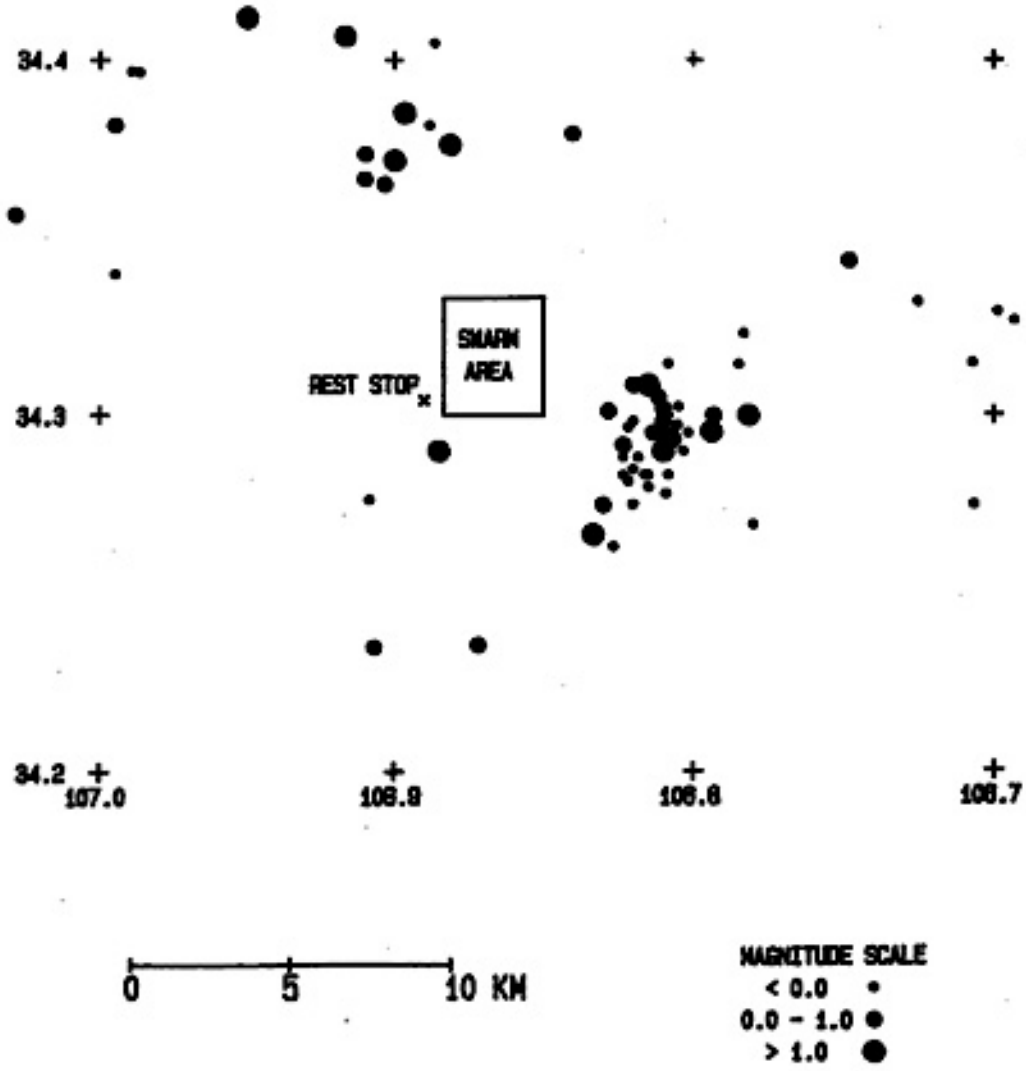

Figure 6. Earthquake epicenters in the vicinity of the Rest Stop Swarm located by the USGS-NMT array between January, 1982 and February 24, 1983. The 2 s.d. errors in the epicenters are approximately 1 km.

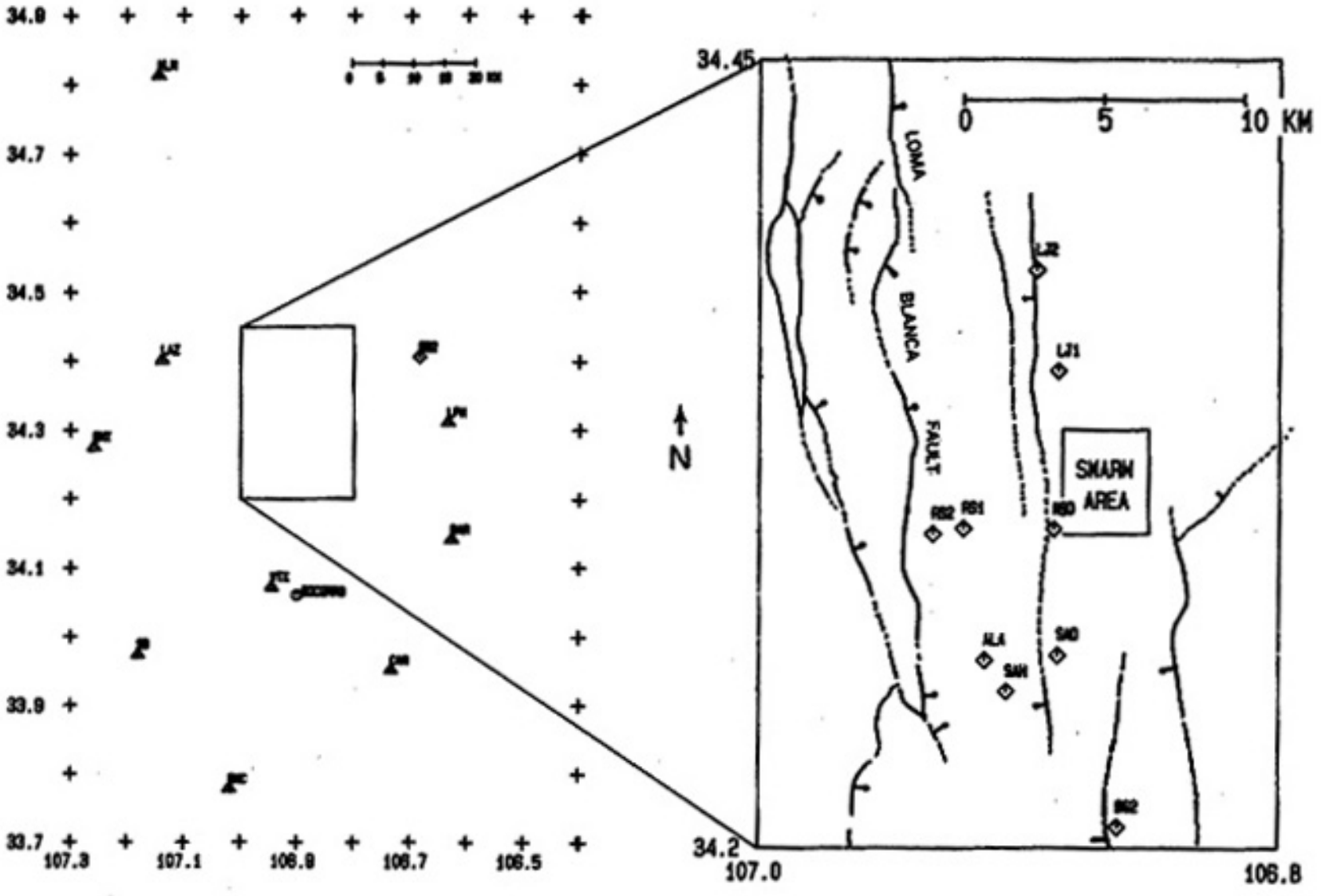

Figure 7. Locations of permanent (triangles) and temporary (diamonds) stations and the surface traces of mapped faults in the Rest Stop Swarm area (from Machette and McGimsey, 1983).

DATA ACQUISITION AND ANALYSIS

Seismograph Stations

The principal data set for this study consisted of analog short-period seismograms from both permanent and temporary seismograph stations. These records provided arrival time and first motion information that was used to count and locate the earthquakes and to determine their focal mechanisms.

Permanent Stations

An array of eight permanent stations made up the NMIMT-USGS Socorro area network at the time of the swarm. Table 1 contains the locations and elevations of the permanent stations. The locations of the permanent stations are indicated by triangles on Figure 7. The seismic signals for the network are telemetered from the remote stations to the observatory on the NMIMT campus where they are recorded by helicorders at 60 mm/min. These stations, which operated during the entire swarm, provided P-wave arrival times and first motions, some S-wave arrival times, and duration times for calculating magnitudes. The timing system for these stations is located at the observatory. Clock drift, which was corrected each day, ranged from 0.042 to 0.053 seconds per 24 hours. The arrival times were not corrected for clock drift, since the measurement error was larger than the error introduced by the clock drift.

Appendix 1 contains a typical response curve from one

Table 1. Locations and Elevations of the Permanent and Temporary Seismograph Stations.

Station	Latitude (N) (degrees)	Longitude (W) (degrees)	Elevation (meters)
PERMANENT STATIONS			
BAR	34.1420	107.6280	2120
BMT	34.2750	107.2602	1975
CAR	33.9525	107.7345	1618
LAZ	34.4020	107.1393	1853
LPM	34.3128	106.6338	1707
MLM	34.8142	107.1450	2088
SB	34.9752	107.1807	3230
SMC	33.7787	107.0193	1560
WTX	34.0722	106.9458	1555
TEMPORARY STATIONS			
SAH	34.2500	106.9055	1414
RSD	34.3032	106.8872	1481
ALA	34.2602	106.9133	1420
LJ1	34.3520	106.8852	1481
BB2	34.4070	106.6837	1567
SAD	34.2628	106.8858	1433
RS1	34.3023	106.9220	1475
BG2	34.2068	106.8632	1475
LJ2	34.3837	106.8938	1512
RS2	34.3013	106.9340	1494

Table 2. Types of Instruments and Periods of Operation for the Temporary Seismograph Stations.

Station	Type of Seismograph	Period of Operation (UT)
SAH	MEQ-800	March 3 0415 to March 3 1900
RSD	MEQ-800	March 3 0450 to March 11 2200
ALA	Portacorder	March 3 1450 to March 6 1700
LJ1	Portacorder	March 3 1530 to March 8 1700
SAD	MEQ-800	March 3 2230 to March 4 2030
BB2	Portacorder	March 3 2315 to March 6 1700
RS1	Portacorder	March 6 1800 to March 8 1700
BG2	Portacorder	March 7 2100 to March 9 2000
LJ2	Portacorder	March 8 1800 to March 11 1700
RS2	Portacorder	March 9 1800 to March 11 1900

of the stations in the permanent array. For a more detailed discussion of the frequency response of these stations, see Ake (1984).

Temporary Stations

An array of temporary stations was deployed shortly after the magnitude 4.0 earthquake. It consisted of one station a few kilometers from the epicentral region that operated almost to the end of the swarm, and two to four portable units that occupied 11 different sites between 4 and 20 km from the epicentral region. The portable units included both Sprengnether MEQ-800 seismographs recording on smoked paper and Geotech Portacorder seismographs recording with ink. All of the portable units operated at 120 mm/min, and their internal clocks were compared with WWV at least every other day to determine clock error and drift, which were used to correct the arrival times. The only information used from the temporary stations was P-wave arrival times and first motions. Table 1 lists the locations and elevations for the temporary stations, and Table 2 lists the interval of operation and type of instrument for each of the stations. Figure 7 shows the locations of the temporary stations.

In Appendix 1 is a typical response curve from one of the portable seismograph units.

Other Stations

Short-period records from an array of stations in northern New Mexico operated by the Los Alamos National

Laboratory provided first motion information for a few of the largest shocks in the swarm.

The Albuquerque Seismological Laboratory provided short-period and Wood-Anderson records for the day of the main shock.

Earthquake Location Procedure

Sixty-seven of the RSS earthquakes were located using the location algorithm HYPO71 (Lee and Lahr, 1975). Following is a description of the location procedure including arrival time weighting, crustal model, the procedure used to establish the station corrections, and the quality of the resulting locations.

Arrival Time Weighting

The P-wave arrivals were timed to within +/- 0.05 sec. A problem arises here because the estimated error in the arrival times for the permanent stations was about 0.08 seconds, whereas the estimated error for the temporary stations was about 0.03 seconds. To compensate for this, the arrivals from events with both types of records were weighted according to type of record as well as quality. The weighting was on a scale of 0 to 3; clear, impulsive arrivals were assigned weights of 0 if they were from temporary stations and weights of 1 if they were from permanent stations. Poorer arrivals were weighted less heavily, according to their quality; very poor arrivals were given weights of 3. For events with readings from only the

permanent station array, clear, impulsive arrivals were weighted 0, and poorer arrivals were given weights between 1 and 3. Very few S-wave times were used; all were assigned weights of 3.

Crustal Model

The location program HYPO71 (Revised) (Lee and Lahr, 1975) was used for all of the earthquake locations. The crustal model was a homogeneous half-space with a P-wave velocity of 5.85 km/sec and a Poisson's ratio of 0.25. Justification for this model is given by Rinehart (1979) and Ward (1980).

Station Corrections

The simplicity of the crustal model was compensated for by using an iterative process to obtain station corrections specifically for events in the RSS area. Twenty-eight large events that occurred when at least four of the close-in temporary stations were operating were selected. Events in this data set all produced clear arrivals at most of the permanent stations. The station corrections for all of the stations were set to zero, and the entire group was located with HYPO71. The station correction for each station was then set to the average of the 28 residuals at that station, and the whole group was run again. The process was repeated four times, until most of the average residuals were less than the estimated measurement errors in the arrival times.

Table 3 lists the final corrections, the number of readings used to arrive at each correction, and the average

Table 3. Final Station Corrections for the Seismograph Array (Also listed are the number of readings used to determine each correction, the average residual for the final calibration run, and the standard deviation of the average residual).

Station	Correction (delay, sec.)	Number of readings	Average residual	Standard deviation
BAR	0.00	28	-0.03	0.05
BMT	0.01	28	-0.01	0.07
CAR	0.12	28	-0.01	0.07
LAZ	-0.07	27	-0.01	0.04
LPM	-0.06	28	0.01	0.04
MLM	-0.10	5	0.05	0.08
SMC	0.03	21	0.02	0.09
WTX	-0.04	25	0.03	0.14
RSD	-0.25	26	-0.04	0.07
ALA	0.14	13	0.00	0.07
LJ1	0.11	19	0.01	0.06
BB2	0.13	11	0.03	0.04
SAD	-0.10	8	0.03	0.05
RS1	0.06	6	0.04	0.02
BG2	0.05	7	0.02	0.03
LJ2	0.64	6	0.04	0.04
RS2	0.01	4	0.01	0.02

and standard deviations of the residuals for the final run of the 28 events. These corrections are delay times, i.e., they are subtracted from the observed arrival times. If a station correction is positive, the average velocity of the travel path to that station is less than the assumed velocity (5.85 km/sec in this case). This would be the case if the station was sitting on top of thick, low velocity sediments. The station correction would be negative if the station was sitting directly on high-velocity material.

The purpose of the procedure described above was to "calibrate" the station array for events in the swarm area by using a group of master events with good depth control (several stations with epicentral distances less than the focal depth) and small gaps ($< 100^{\circ}$). The resulting station corrections arise from differences between the assumed and true velocities along the entire travel paths, thus making the particular choice of velocity model less critical. Of course, the major differences between the assumed (5.85 km/sec) and true velocities occur in the upper few kilometers beneath the stations.

Variable-Depth Solutions

From the entire swarm, 67 earthquakes were large enough ($M_L > 0.5$) to have sufficient readings (at least 5) to be located well by HYPO71. Of the 67 solutions, 10 were quality A, 26 were quality B, 24 were quality C, and 7 were D quality. For a discussion of the criteria that HYPO71

uses to arrive at the quality factors, see Ake (1984). The 7 D quality locations were not considered further. Eighteen of the B quality solutions were given that designation by HYPO71 only because their gaps were higher (< 20°) than the 90 degree cutoff between A and B solutions. These events had readings from at least two of the close-in temporary stations, and small RMS errors. The 18 events are included with the 10 A quality solutions in a high-quality data set that was used to examine the depths of focus.

Two of the outputs of HYPO71 for each solution are erh, the estimate of epicentral error, and erz, the estimate of focal depth error. Both erh and erz represent approximately twice the standard deviation of their respective parameters. (Lahr, personal communication). For the 28 high quality solutions, the average erh was 0.4 (+/- 0.1 s.d.) km and the average erz was 0.6 (+/- 0.2 s.d.) km.

Fixed-Depth Solutions

Because the majority of the swarm's earthquakes occurred when no close stations were operating, and hence the depths of focus were poorly constrained, an attempt was made to obtain good epicenters for these events by fixing their depth at the average depth for the 28 well-constrained hypocenters, which was 6.5 (+/- 0.9 s.d.) km. All of the swarm events with at least six P-wave arrival time readings and a local magnitude greater than 0.5 were located with the depth fixed. The 28 events with close-in stations were included in this group, but only the permanent stations were

used for all of the fixed-depth solutions in order to eliminate biases in the locations due to different station distributions. The result was 60 solutions with an average erh of 0.8 (+/- 0.9 s.d.) km.

Output Parameters

Appendix 2 contains a sample of the HYPO71 output for one of the swarm events, as well as a table of HYPO71 output parameters for the 28 high-quality solutions and the 60 fixed-depth solutions.

Magnitude Calculation

Local magnitudes for the swarm events were computed from measurements of signal duration on short-period seismograms using the LANL duration magnitude formula (Newton and others, 1976):

$$M_L = 2.79\log(\text{duration}) - 3.63. \qquad (1)$$

This relationship was found to be applicable to the central Rio Grande rift for earthquakes with magnitudes greater than about 1.0 by Ake and others (1983). The duration-based magnitude formula underestimates the magnitudes of smaller earthquakes relative to amplitude-based magnitudes.

RESULTS

Characteristics of Main Shock

On approximately the sixth day of the swarm, on March 2 at 23:22 UT (4:22 MST), the main shock of the swarm occurred. It had a local magnitude based on duration of 4.0, and was felt over a relatively large area (7000 km^2). The earthquake was felt as far away as Mountainair, 65 km to the northeast. Ten eyewitness reports from people who were within 5 km of the epicenter indicate an intensity of V-VI on the Modified Mercalli Intensity Scale, i.e., felt by everyone, some instances of cracked plaster, objects knocked off shelves, etc. In Socorro, 28 km to the south of the epicenter, many witnesses reported an intensity of about III-IV (felt noticeably indoors), as did five persons from Bosque, which is about 30 km to the north of the epicenter. The intensity dropped to I (felt by only a few) at Belen and San Antonio, which are 42 kilometers north and 45 kilometers south, respectively.

An interesting observation from the distribution of felt reports is that the shock was felt much farther to the east than it was to the north. The earthquake was felt in Mountainair, 65 km to the northeast, but was felt no farther north than Belen, about 42 km to the north. The best explanation for this phenomenon is that P and S waves are more severely attenuated along travel paths that lie solely within the Rio Grande rift than for paths that are mostly

outside the rift.

General Swarm Characteristics

The time distribution of the number of earthquakes, the time distribution of energy release, and the relationship between the log of the cumulative number of earthquakes and local magnitude were determined for the swarm. The data set for these studies was a tabulation of times and durations for events with durations greater than or equal to 20 seconds (M_L=0.0) at station BAR between February 25 and March 17, 1983. These dates for the beginning and end of the swarm were chosen because there was no significant activity in the RSS area in the 7 days before February 25 and the 7 days after March 17.

Figure 8 is a histogram of the number of earthquakes in each 2-hour period during the swarm. The most notable feature of this plot is the 48-hour quiet period preceding the main shock. Only two moderate earthquakes occurred during this interval, at 18:05 (M_L=1.2) and 18:14 (M_L=1.0) on March 2, about five hours before the main shock at 23:22.

Figure 9 is a histogram relating the log of energy release to time. The energy released by each earthquake was calculated using Richter's (1958) relationship between local magnitude and energy release. The appearance of the time-energy plot is similar to the time-number plot of Figure 8. Most of the energy for the swarm was released by the main shock and the aftershocks during the following 48 hours.

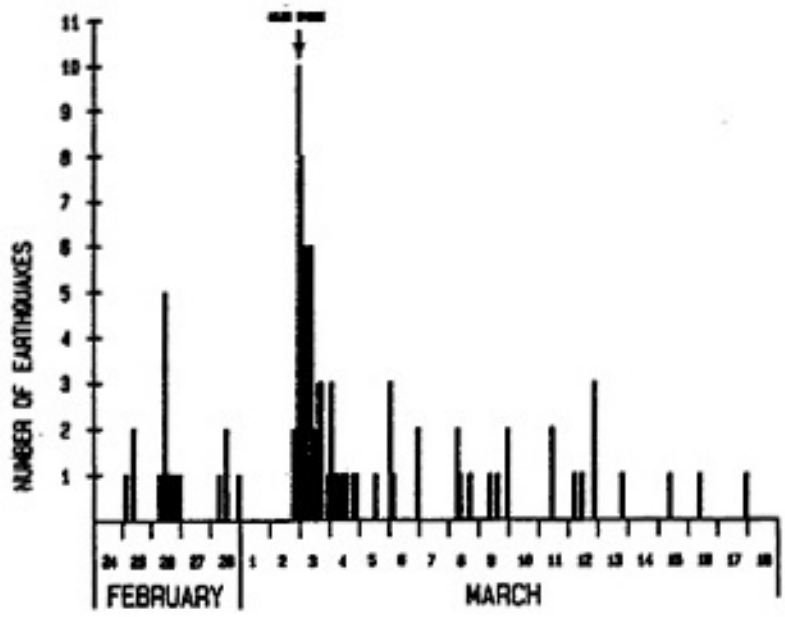

Figure 8. Histogram of the number of earthquakes with $M_L \geq 0.0$ as a function of time for the Rest Stop Swarm. Each interval is two hours, and the time of the main shock (March 2, 23:22) is indicated.

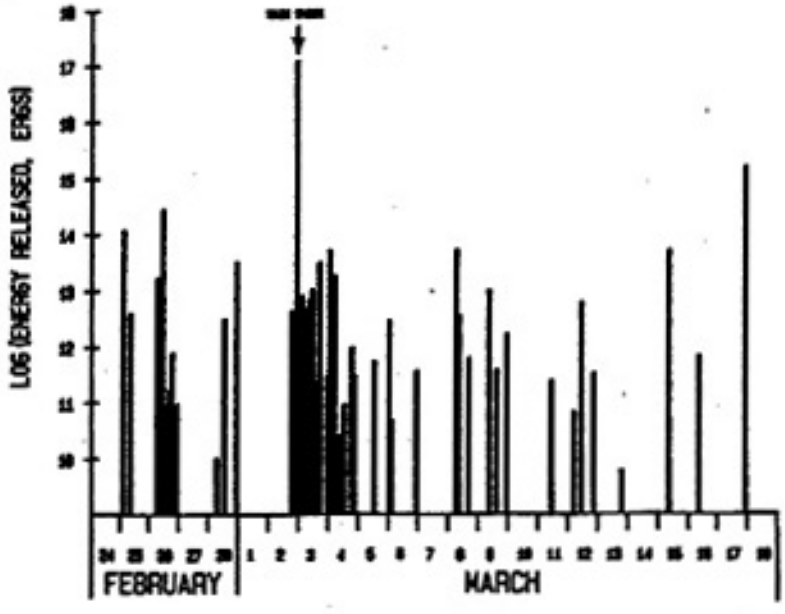

Figure 9. Histogram of the log of the energy release as a function of time for Rest Stop Swarm earthquakes with $M_L \geq 0.0$ The energy released in each two hour period was calculated using Richter's (1958) relationship between local magnitude and energy.

After that, the activity dropped to about the same level as before the main shock.

Figure 10 shows the relationship between local magnitude and the log of the cumulative number of earthquakes. It appears from the plot that the data set is complete for the 73 events with magnitude greater than 1.0. Linear regression for all of the events with magnitudes between 1.0 and 2.5 results in the relationship:

$$\text{Log } \Sigma N = 2.34 - 0.78 M_L . \qquad (2)$$

The above relationship predicts that the largest event in the swarm should have a magnitude of slightly more than 3.0, i.e., the intercept of the magnitude axis is 3.15.

Epicenters

Figure 11 is a map view of the locations of 60 events from the entire swarm period obtained by fixing the depth at 6.5 km. The area defined by the epicenters is about 2.5 by 4 km, or 10 km^2.

Figures 12 and 13 are perhaps more meaningful than Figure 11; only events that had local magnitudes greater than or equal to 1.0 and erh less than or equal to 0.5 km are plotted in these figures. The circle around each symbol has a radius equal to the erh for that location. Figure 12 shows the location of the main shock along with eight foreshocks, and Figure 13 shows the location of the main

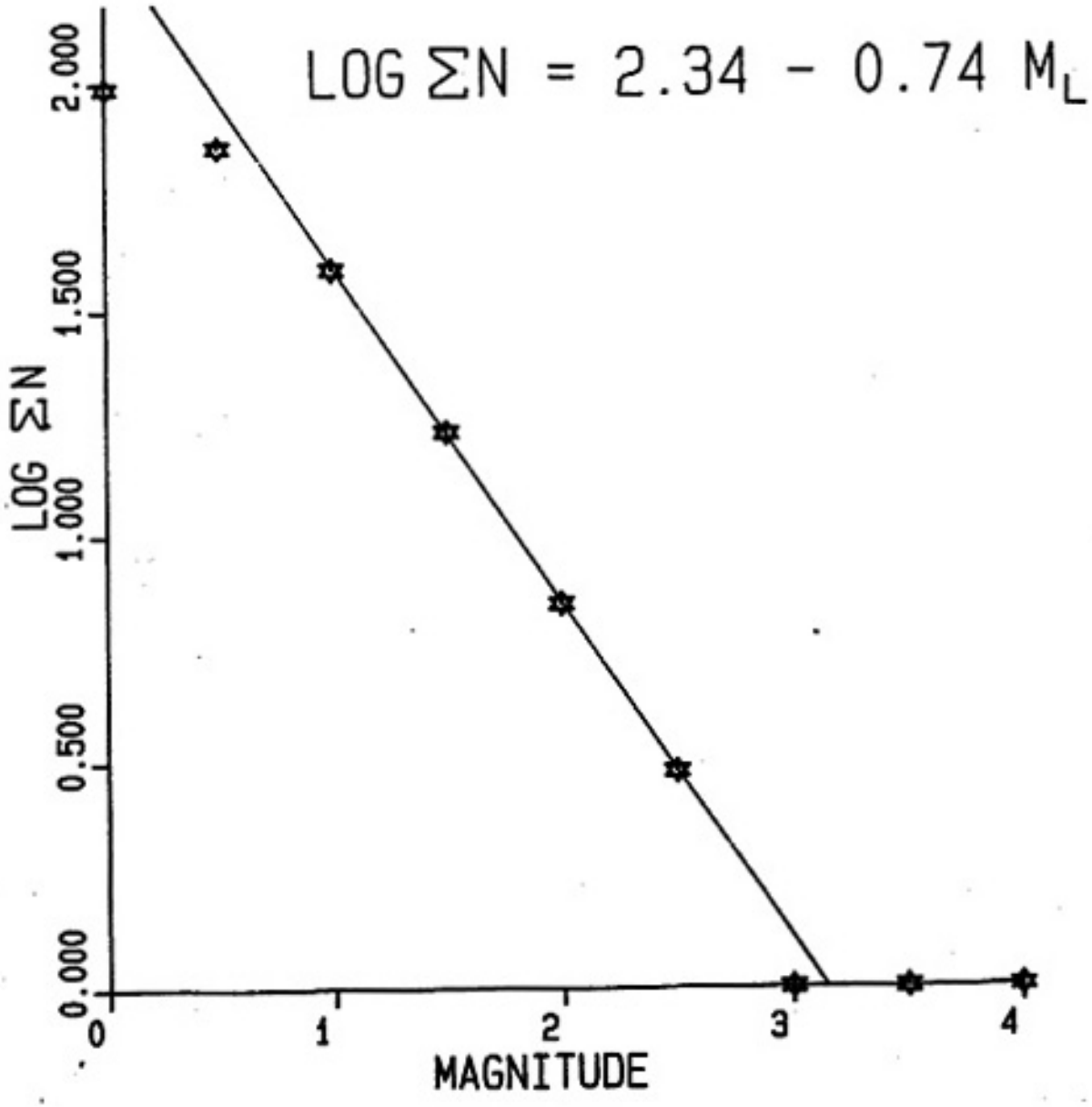

Figure 10. Plot of the relationship between the log of the cumulative number of earthquakes and magnitude for 97 Rest Stop Swarm events with $M_L \geq 0.0$. The line is a least-squares fit to the four points with magnitudes between 1.0 and 2.5.

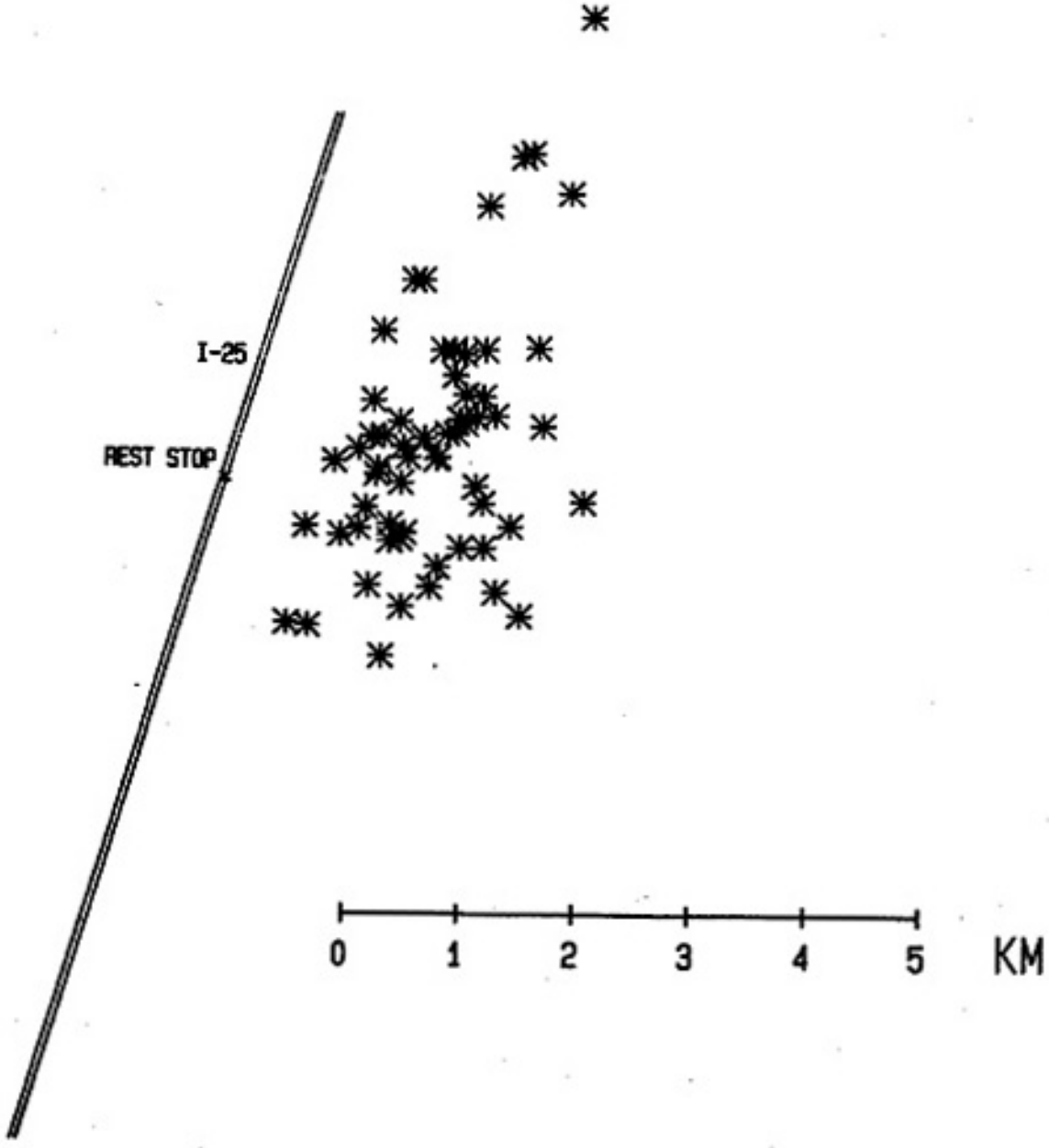

Figure 11. Epicenters for 60 earthquakes with magnitudes greater than 0.5 from the entire swarm period. The average epicentral error (erh) is about 0.8 km (2 s.d.).

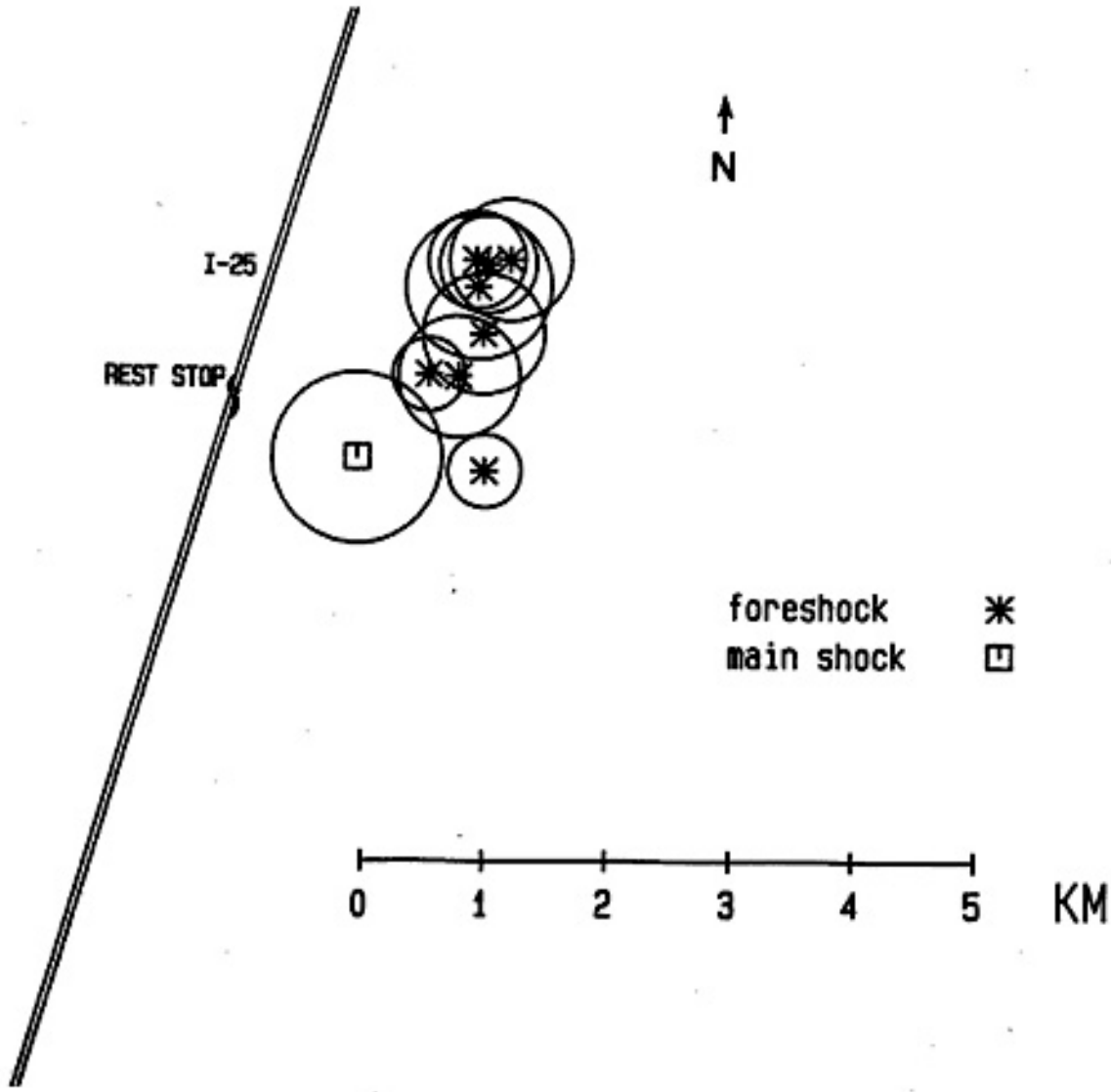

Figure 12. Epicenters of eight foreshocks and the main shock. Each circle has a radius equal to erh, the 2 s.d. estimate of the epicentral error for that location.

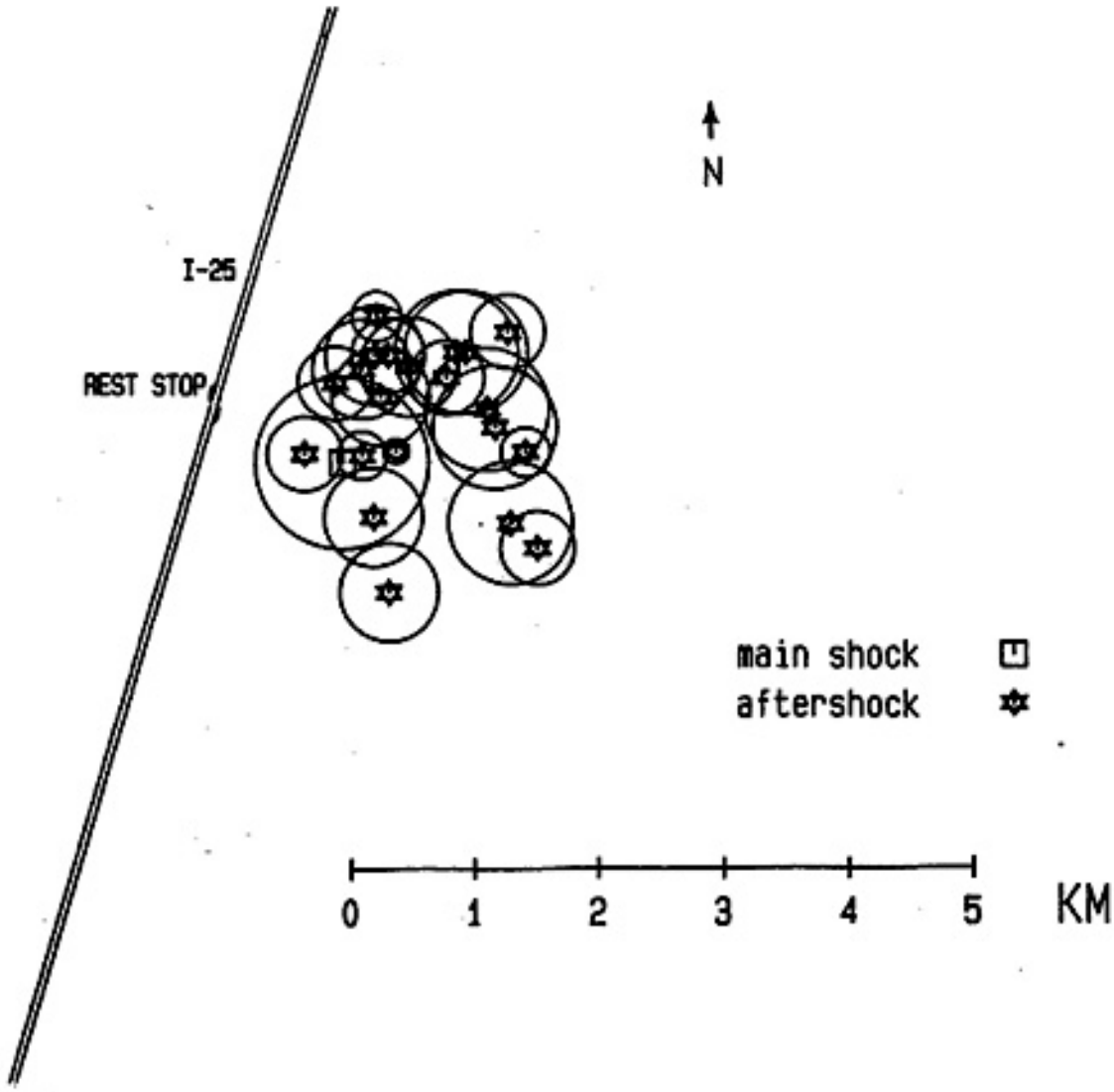

Figure 13. Epicenters of 21 aftershocks and the main shock of the Rest Stop Swarm. The radius of each circle is equal to erh, the 2 s.d. estimate of epicentral error.

shock with 21 aftershocks. For the most part, the aftershocks tended to cluster closely around the main shock, with some possible migration to the east. The foreshocks, on the other hand, seemed to trend more toward the north and east of the main shock. Examination of Figures 12 and 13 indicates that the amount of area affected by the earthquakes is as large as Figure 11 suggests, because the large and well-located events plotted in Figures 12 and 13 involve about the same area as the total data set of Figure 11.

To determine the migration of the foreshocks with time, Figure 14 was plotted with epicenters of Figure 12 indicated by numbers corresponding to their time sequence. There appears to be no consistent pattern in the movement of epicenters with time.

Hypocenters

The hypocenters of the 28 aftershocks with high quality solutions were plotted on vertical sections with orientations between 0 and 180 degrees, at 20 degree intervals. The cross-sections are shown in Figure 15. For each cross-section, the hypocenters have been projected onto a vertical plane with strike equal to the angle indicated (degrees clockwise from north). Each symbol's vertical length is equal to the error in the depth of focus (erz), and each symbol's horizontal length is erh.

It appears that the cross-sections with orientations of 60° and 120° show the "best" alignment of the hypocenters.

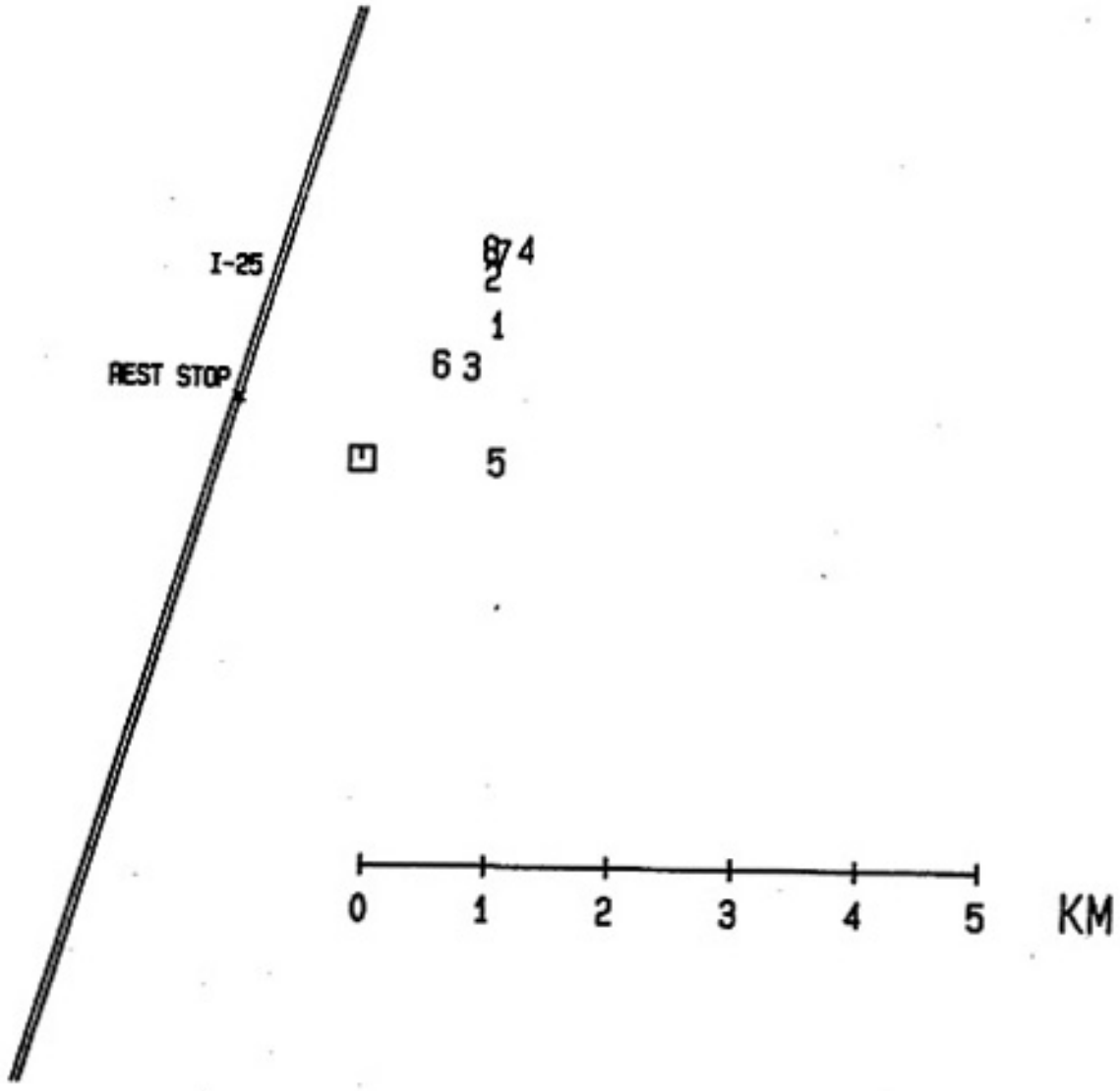

Figure 14. Epicenters of Figure 12 denoted by numbers that signify the time sequence of the occurrence of the earthquakes.

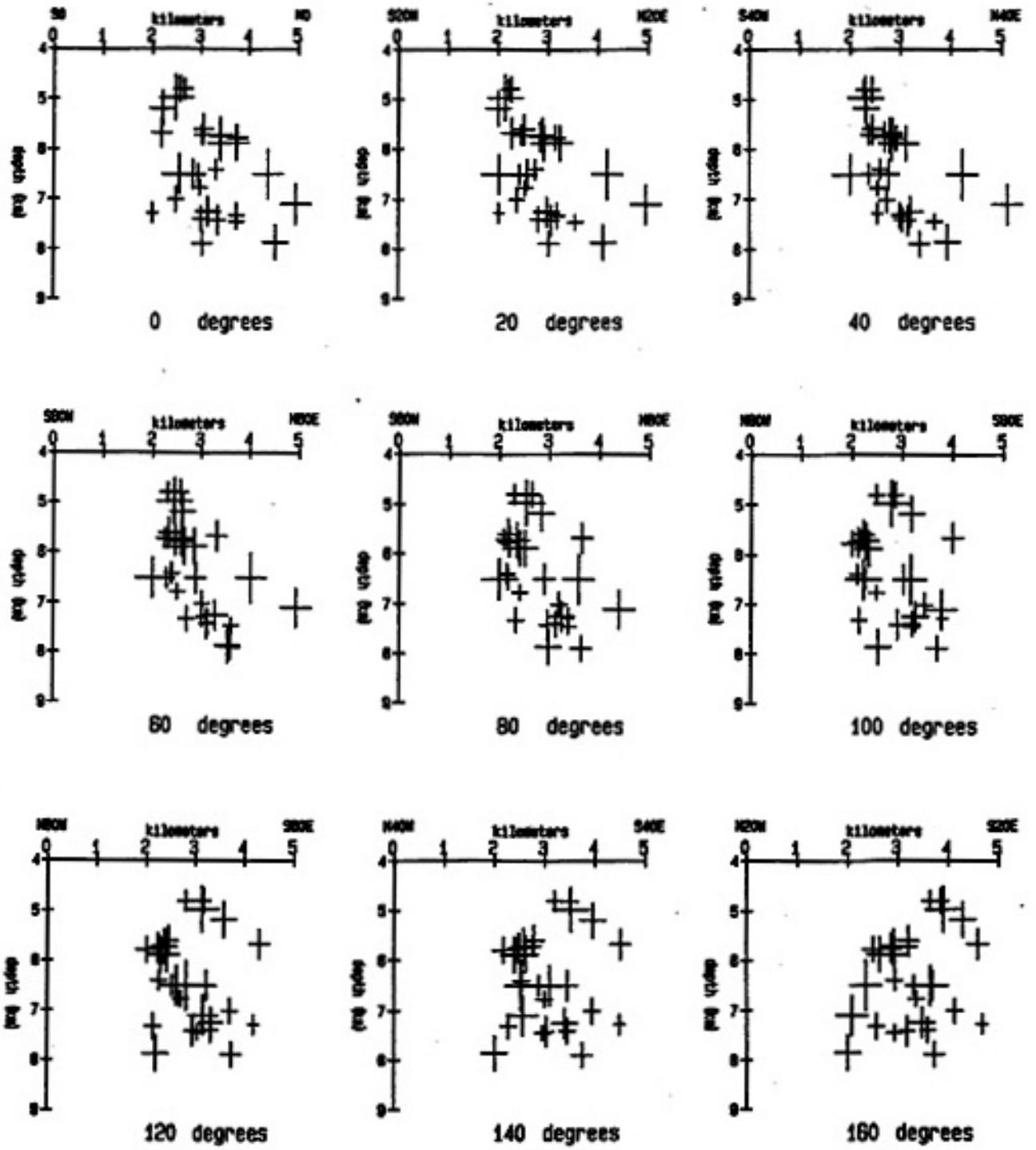

Figure 15. Vertical sections showing the 28 high-quality hypocenters. The strike of the cross-sections, measured clockwise from north, are given beneath the figures. The horizontal length of each symbol is equal to erh, the 2 s.d. estimate of the epicentral error, and the vertical length is erz, the 2 s.d. estimate of the error in the depth of focus.

Examination of cross-sections at angles of 50° and 70° and angles of 110° and 130° indicates that the best alignment occurs for the cross-sections with orientations of 65 and 115 degrees. Figure 16 shows the two cross-sections (65° and 115°) with lines indicating the projections of the planes passing through the majority of the hypocenters. It is apparent that there is considerable variability in both the dips and strikes of these planes. However, to a first approximation, one of the planes strikes about N25°W and dips 60 degrees to the northeast, and the other plane strikes N25°E and dips 50 degrees to the southeast.

Figure 17 is a histogram of the depths of focus for the 28 high quality solutions. The depth interval is 0.5 km, slightly less than the the average erz (0.6 +/- 0.2 s.d.) km for these hypocenters. The depths range from about 4.5 km to about 8.5 km, with the largest numbers between 5.5 and 6.0 km, and between 7.0 and 7.5 km. The mean depth of focus for the 28 earthquakes is 6.5 (+/- 0.9 s.d.) km.

Examination of the distribution of aftershock hypocenters and their associated errors indicates that the volume of crust involved could range between a minimum of 3 km^3 and a maximum of 12 km^3. If the earthquakes are assumed to lie along a plane, the area of the planar region defined by the aftershocks is about 9 km^2.

Focal Mechanisms

An attempt was made to determine the focal mechanisms

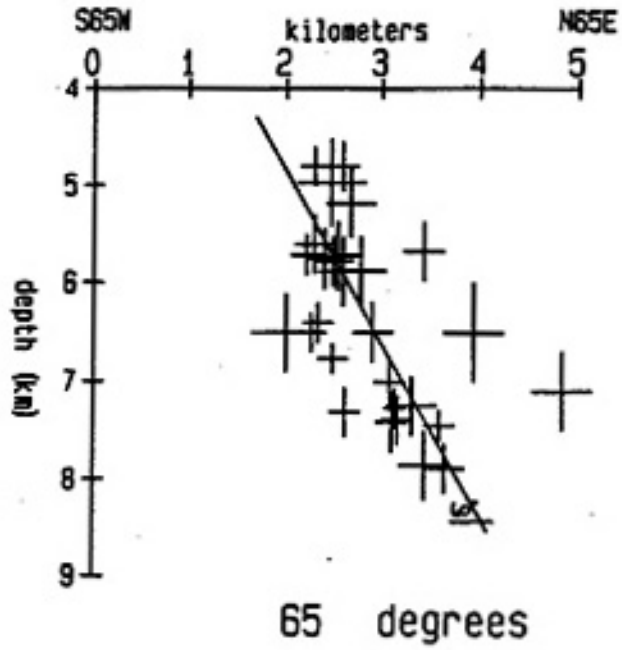

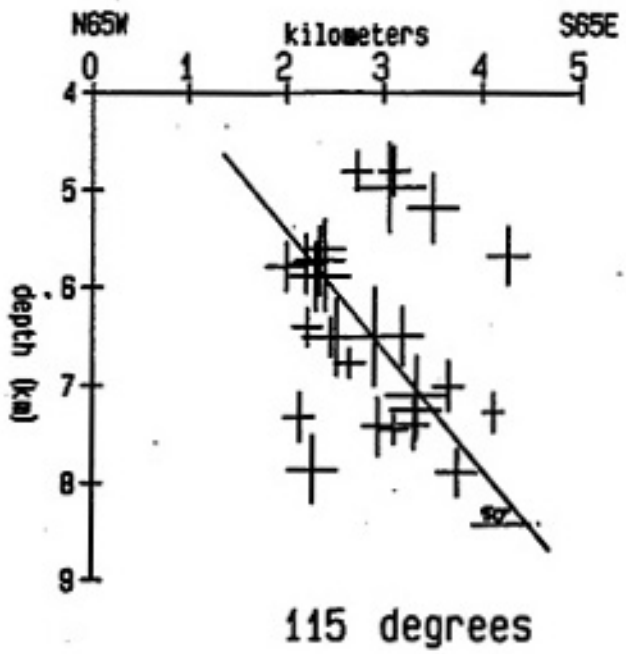

Figure 16. The vertical sections exhibiting the best alignment of the 28 hypocenters. The two planes defined by the hypocenters are shown by the lines; the plane in the top diagram strikes N25W and dips 60 degrees to the east, and the plane inferred by the bottom diagram strikes N25E and dips 50 degrees to the east.

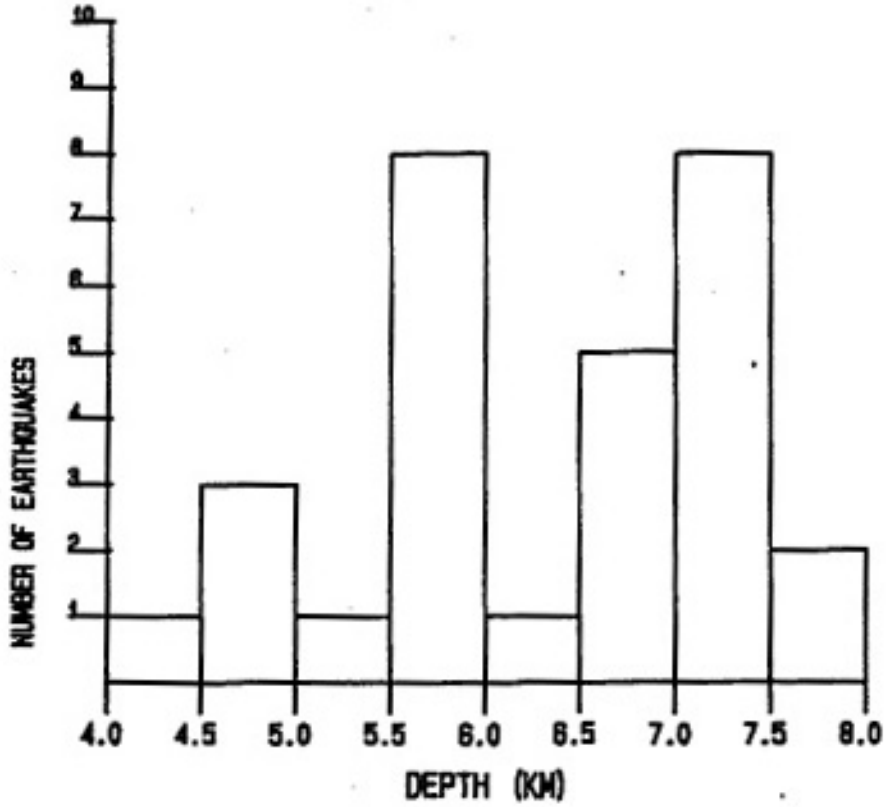

Figure 17. Histogram of the depths of focus for the 28 high-quality solutions. The average error in the the depth (erz) is about 0.6 km (2 s.d.)

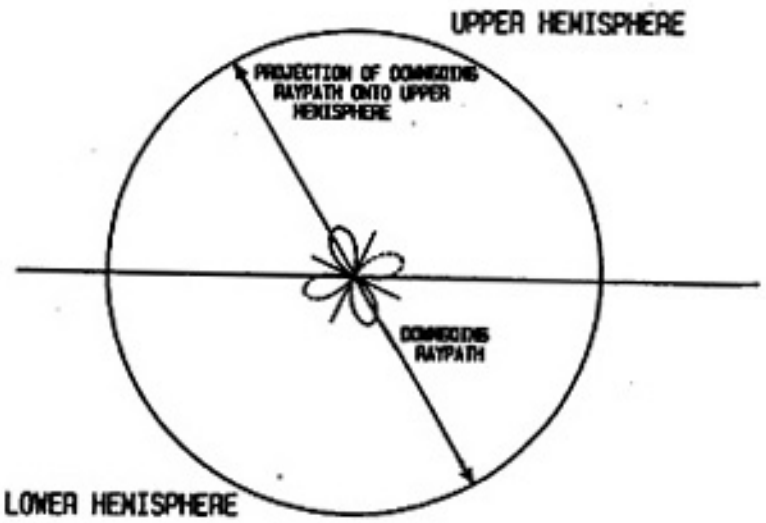

Figure 18. The procedure used to project downgoing raypaths onto the upper focal sphere.

for some of the individual events in the swarm. The distributions of first motions were plotted on stereographic projections. Some of the earthquakes, including the main shock, yielded conventional fault plane solutions in general agreement with previous results from the same area (Wieder, 1981; and Sanford and others, 1979) but many of the focal mechanisms could not be explained by the conventional double-couple model of faulting.

First Motion Data

The polarities of the permanent stations were determined from strong explosions and from teleseisms with known first motions. The polarities of the MEQ-800s were normal, i.e., "up" was a compression and "down" was a dilatation. The polarities of the Portacorder units were also found to be normal, from the first motions of explosions.

Since most of the first motions were direct P arrivals, the first motions were plotted on the upper focal sphere. For these arrivals, straight raypaths were assumed. Several distant stations were also used. However, for these, the first arrivals were either Pn (conical wave generated in the upper mantle) or P* (conical wave generated just beneath the mid-crustal Conrad discontinuity) arrivals. The procedure used to correct for the fact that the Pn and P* arrivals should have been plotted on the lower focal sphere is illustrated in Figure 18. To determine the take-off angle

for Pn and P*, a velocity of 6.5 km/sec was used for the material beneath the Conrad discontinuity, which is at about 19 km depth, and a velocity of 8.1 km/sec was used for the upper mantle.

Focal Plane Solution of Main Shock

Figure 19 is an upper focal sphere stereographic projection of the first motions of the main shock and the nodal planes for a standard douple-couple fault plane solution. For each of the nodal planes, three planes are drawn. The center plane is the best fit to the data, and the outside planes represent the limiting cases that the data allow. One nodal plane has a strike of N15°W and dips 50 degrees to the west. The other nodal plane strikes N22°E and dips 46 degrees to the east. The inferred fault motion is primarily normal dip-slip, with a small right-lateral strike-slip component. In general, the focal mechanism suggests normal faulting on a north-northeast or north-northwest striking plane that dips about 50 degrees.

Constraints on Focal Mechanism of Main Shock

One constraint on the possible focal mechanism of the main shock arises from the possibility that the aftershocks occurred on the fault plane of the main shock. If the well-located hypocenters of the aftershocks lined up on one of the two possible fault planes, then that plane would be the preferred fault plane. Figure 20 is a stereographic projection of the two possible fault planes (solid) along with the two planes defined by the hypocenters (dashed). On the basis of this argument, the northeastward striking,

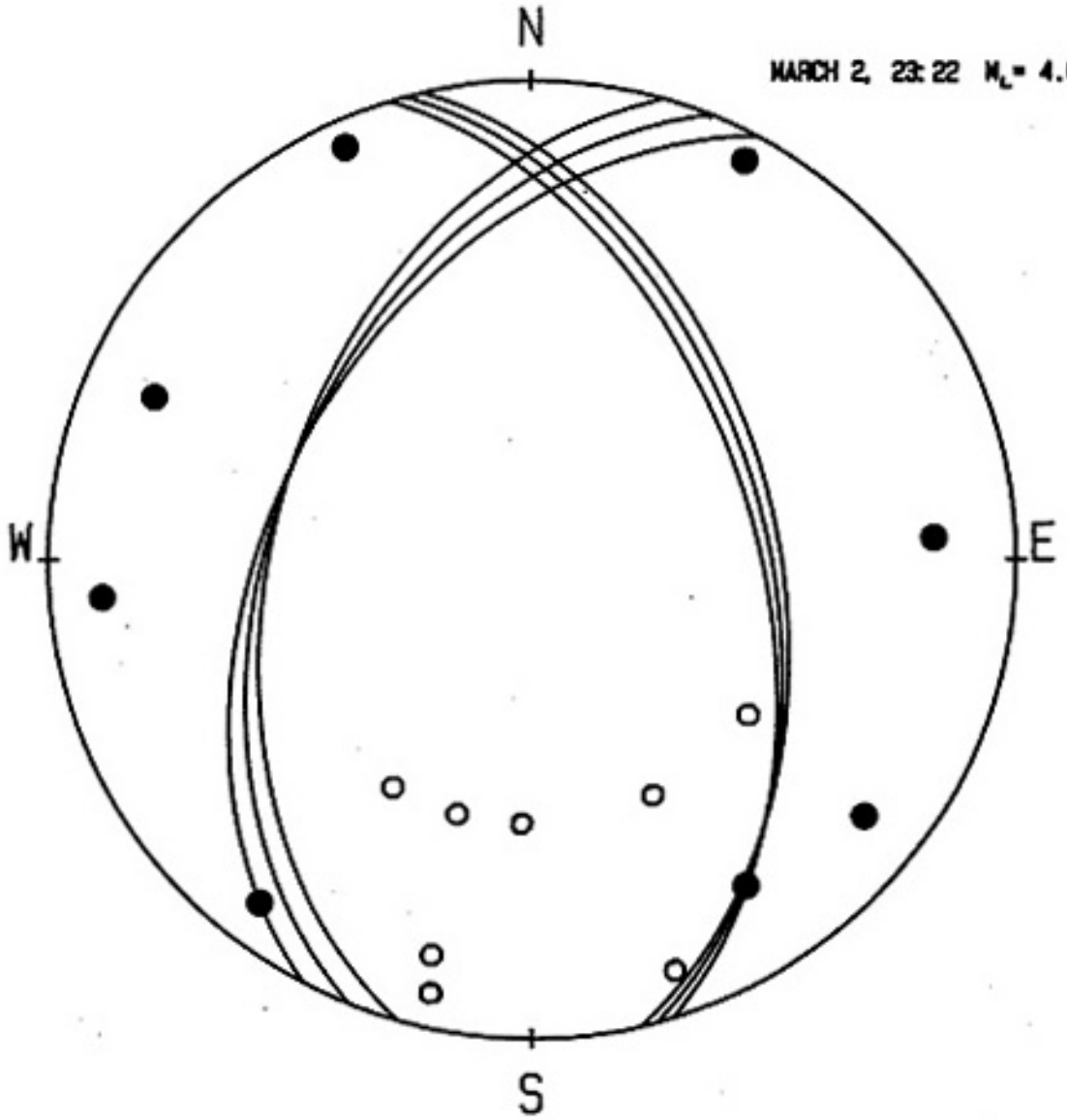

Figure 19. Upper focal sphere projection of P-wave first motions for the main shock. Open circles represent dilatations and dark circles are compressions. The nodal planes drawn are for the standard double-couple model of faulting. The center plane is the best fit to the data, and the outside planes are the limiting orientations of the nodal planes allowed by the data.

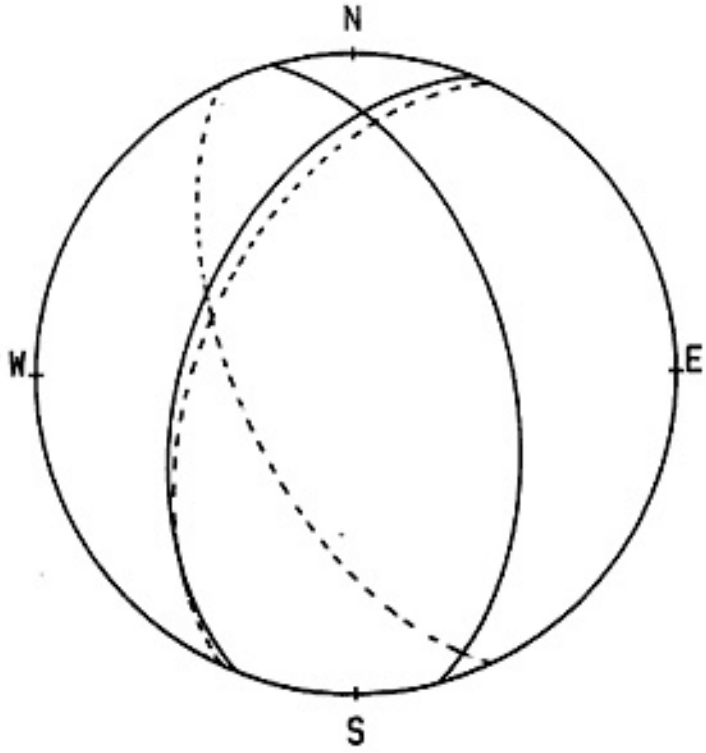

Figure 20. Upper hemisphere projections of the nodal planes of the main shock (solid) and the planes defined by the hypocenters (dashed) from Figure 16.

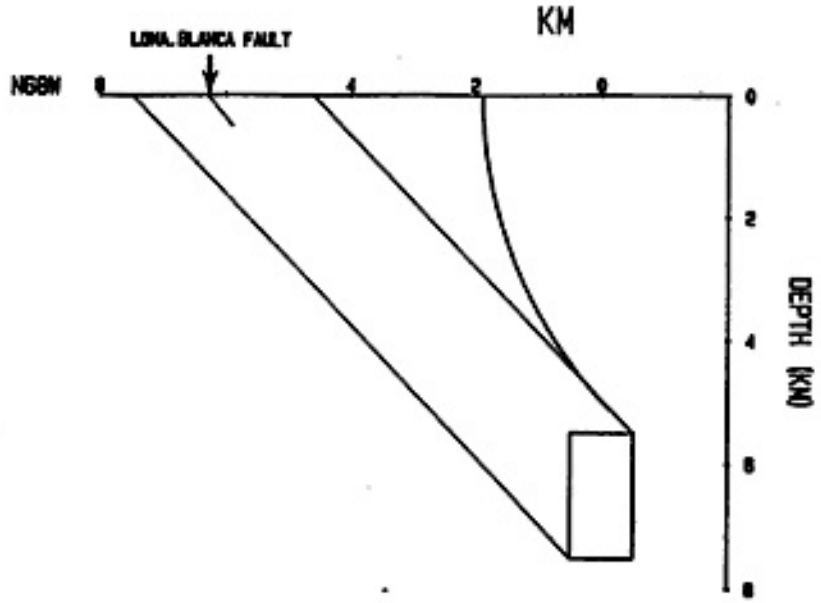

Figure 21. Cross-section showing the projections of one of the nodal planes of the main shock (from Figure 19) assuming both planar and listric faulting. The estimated error in the location of the main shock has been taken into account.

southeastward dipping fault plane is the best choice because the hypocenters of the aftershocks more closely lie along that plane.

The preferred nodal plane of the main shock, as determined by the distribution of the aftershocks, was projected to the surface to see whether a correlation with surface faults could be found. Figure 21 is a cross-section perpendicular to the strike of the eastward dipping nodal plane showing the projection of the plane to the surface assuming both planar and listric faulting. Also shown is the position of a major mapped surface fault, which has a roughly northerly strike. The location of the main shock is represented by a rectangular area that takes into account the error in the location. The curving fault plane is the limiting listric fault; listric faults could occupy the area between this curve and the westernmost planar projection. The two straight lines delineate the area that the projection of a planar fault could occupy. If the projection of the nodal plane is planar, it could intersect with the Loma Blanca fault at the surface.

First Motion Diagram for One Foreshock

One of the shocks that occurred before the the main shock (Feb. 26, 11:15, M_L= 2.5) was large enough to produce good first arrivals at the Los Alamos stations as well as the NMIMT-USGS network stations. The distribution of first motions for this earthquake is shown by Figure 22. A double-couple fault plane solution could not be made to fit

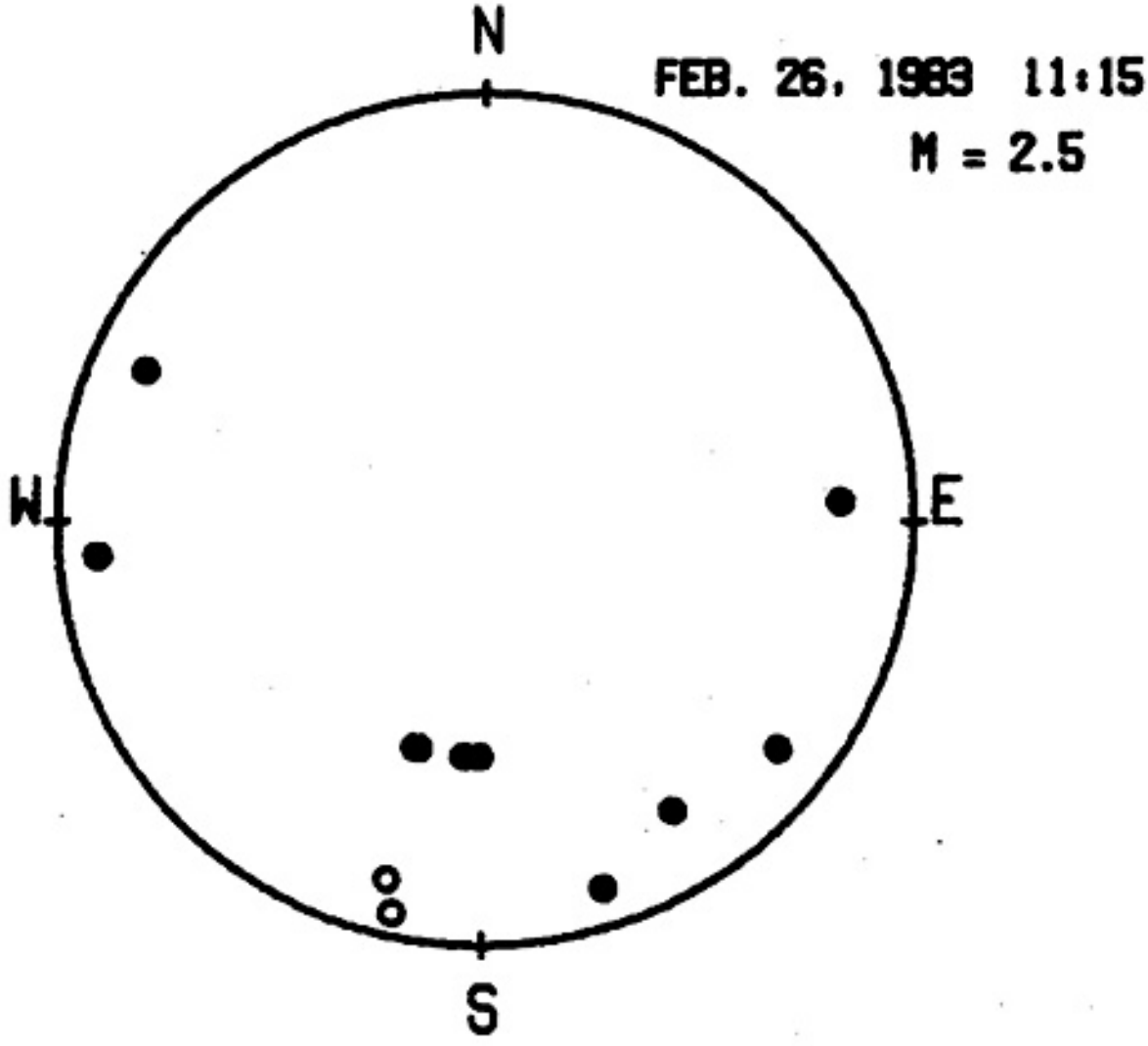

Figure 22. Upper hemisphere projection of the first motions of the earthquake of February 26, 11:15 U.T.

the distribution of first motions for this foreshock.

First Motion Diagrams for Aftershocks

First motion diagrams for 26 aftershocks are plotted in Appendix 3. The patterns of first motions are representative of all of the aftershocks with magnitudes greater than about 0.5.

Source Characteristics

Data that could be used for an analysis of the source characteristics of fault dimension and stress drop was gathered for some of the aftershocks. The procedure utilized measurements of the first half-pulse width (τ_w) on the high-quality analog records from the temporary stations. The procedure for analyzing the data is described in detail by Ake (1984) and will not be presented here. The measurements can be found in Appendix 4, but no analysis of source characteristics was done.

DISCUSSION

Station Corrections

Examination of the station corrections in Table 3 reveals that most of the stations have reasonable corrections, i.e., the absolute values are less than about 0.15 seconds. Delay times with magnitudes less than about 0.15 seconds can be easily explained by differences in the type of material underneath the stations.

The two stations with corrections more difficult to explain are LJ2 and RSD. LJ2 has a delay time of +0.64 seconds, which implies a very low velocity for the travel path to that station. Station LJ2 is in an area where the sedimentary basin fill deposits are very thick; the rift sediments are thought to be as deep as 4 km in some areas of the central Rio Grande rift. If a velocity of 3.0 km/sec is assumed for these sediments, then a delay of +0.65 seconds would result from a 4 km travel path in the sediments relative to a 4 km travel path in material with the assumed velocity of 5.85 km/sec.

Station RSD has a delay time of -0.25 seconds. This station is also in the center of the rift and sits directly on loose sand, so the large negative delay does not agree with the geological observations in the area. One explanation is that there is a hidden volcanic pipe or thick layer of volcanic material near station RSD that is acting

as a high-velocity conduit for the seismic energy.

Depths of Focus and Volume of Crust

The average depth of focus for the high quality RSS aftershock locations was 6.5 (+/- 0.9 s.d.) km. This is considerably shallower than the average depth from swarms to the south of Socorro [8.8 (+/- 0.4 s.d.) km for the May and July, 1983 swarms and 9.7 (+/- 0.2 s.d.) for the May-June, 1977 swarm]. The range in the depths of focus as indicated by the standard deviations is also larger for the RSS. The deepest of the RSS depths of focus (7.8 km) is even less than the shallowest of the well located hypocenters of the other swarms. The smallest depths of focus for the RSS are 4.8 km, which is significantly less than any depths observed from swarms in the central Rio Grande rift. The volume of crust involved by the RSS is also larger than for any of the previous swarms.

Relationship of Maximum Depths of Focus to Temperature

The maximum depth of the well-located RSS earthquakes, about 8 km, may be related to the temperature at that depth. It is possible that the temperature below that depth is too high for brittle fracture to occur. Chen and Molnar (1983) claim that the limiting temperature for earthquake occurrence is between 250 and 450 degrees Centigrade. This implies that the thermal gradient would have to be between 30 and 55°C/km (assuming 10°C for the surface temperature) for the cutoff depth to be 8 km.

The only deep thermal gradient measurements in the central Rio Grande rift are to the north of the RSS, in the Albuquerque basin. These measurements, taken to a depth of 3 km, are in the range of 32-33°C/km (Reiter, personal communication), which is near the lower limit of the 30-55°C range. Gradient measurements farther south, closer to the RSS, are shallower (160-300 m), and therefore more subject to near-surface interference. The gradients for these shallower measurements are higher, about 40-42°C/km (Reiter and others, 1975), and fall closer to the center of the the 30-55°C/km range. Although the uncertainties in the parameters do not allow any definite conclusions to be made, it does appear that the maximum depth of occurrence of the RSS earthquakes could be related to the temperature at that depth.

Relationship of Main Shock Focal Planes to Surface Faulting

The good agreement between the orientation of the eastward dipping fault plane of the main shock and the orientation of the planes defined by the locations of the 28 high-quality aftershock hypocenters, as illustrated by Figure 20, is good evidence that the fault plane of the main shock is the eastward dipping nodal plane from the first motion analysis. The fact that the same plane can be projected westward to the Loma Blanca fault, which has roughly the same strike and dips eastward also, is another point in favor of the eastward dipping fault plane. The

Loma Blanca fault is a young (< 2 m.y.) normal fault which has been mapped 50 km in a northward direction from San Acacia (Machette and McGimsey, 1983). There are no measurements of dip for the Loma Blanca fault, but it must be noted that the correlation of the fault plane of the RSS earthquakes with the surface fault requires a dip of about 50 degrees for the Loma Blanca fault.

Position of RSS with Respect to Mid-Crustal Magma Body

The RSS occurred over the center of the sill-like mid-crustal magma body, which is thought to be currently inflating because of the ongoing crustal doming centered on the magma body. The crustal deformation associated with inflation of the magma body would tend to produce tensile stresses in the upper crust; the largest of these stresses would be at the center of the crustal doming. These tensile stresses could make it easier for magmatic material to migrate upward, into the upper upper half of the upper crust.

Possible Fault Mechanisms of Aftershocks and Foreshock

From even a cursory examination of the first motion diagrams in Appendix 3 and Figure 22, it is apparent that many of the distributions of first motions cannot be explained by the conventional double couple without moment (DCWM) model of faulting. For the diagrams that can satisfy the DCWM model, the solutions are not well constrained by the data, and in many cases do not agree with the focal

plane solution of the main shock. Table 4 lists all of the events in Appendix 3 and the one in Figure 22 and indicates whether a DCWM solution could be made to fit the first motion data, and if it could, whether or not the DCWM solution agreed in general with that of the main shock.

Fourteen of the first motion diagrams could be made to fit the double couple model, but six of these were not in general agreement with the main shock focal plane solution, i.e., some indicated normal faulting on E-W striking planes, and some indicated strike-slip motion. The remaining thirteen first motion distributions did not allow a solution of the DCWM type.

The unusual first motion distributions are predominately compressions, indeed, two of them (March 4, 05:26 and March 4, 18:20) have no dilatations whatsoever, and the compressions cover both the edges and the center of the focal sphere. (The first motions of the shock of March 4, 05:26 are reproduced in Figure 23.) The first motion distributions of these two shocks do not have enough data coverage to rule out the possibility of areas of dilatation, which would make them similar to the other eleven unusual first motion diagrams; nonetheless, a mechanism other than the DCWM must be operating to produce the first motions for all thirteen of the earthquakes.

Many competing fault mechanisms have been proposed in the literature. Since intrusion of magma is suspected as the cause of the earthquakes, mechanisms that result from

Table 4. Possible Mechanisms of 26 Aftershocks and One Foreshock.

DATE	TIME	M_L	FIRST MOTIONS FIT DCWM MODEL	IN AGREEMENT WITH MAIN SHOCK
Feb. 26	11:15	2.5	NO	
March 3	06:31	1.2	YES	NO
March 3	16:07	1.0	YES	NO
March 3	17:40	1.9	YES	YES
March 3	22:35	1.0	NO	
March 4	00:00	2.0	NO	
March 4	01:47	1.9	NO	
March 4	01:49	1.3	NO	
March 4	03:26	0.7	YES	YES
March 4	05:26	1.9	NO	
March 4	13:53	0.6	YES	YES
March 4	18:20	1.1	NO	
March 4	21:49	0.8	YES	YES
March 6	00:11	1.0	YES	NO
March 6	03:00	0.5	YES	NO
March 6	22:13	0.9	YES	NO
March 6	23:26	0.6	YES	NO
March 8	06:06	1.2	NO	
March 8	06:19	2.0	NO	
March 8	08:27	1.4	YES	YES
March 8	16:04	0.9	YES	YES
March 9	09:05	1.7	NO	
March 9	15:03	0.8	YES	YES
March 9	23:03	0.7	YES	YES
March 9	23:25	1.2	NO	
March 11	11:07	0.6	NO	
March 11	11:46	0.6	NO	

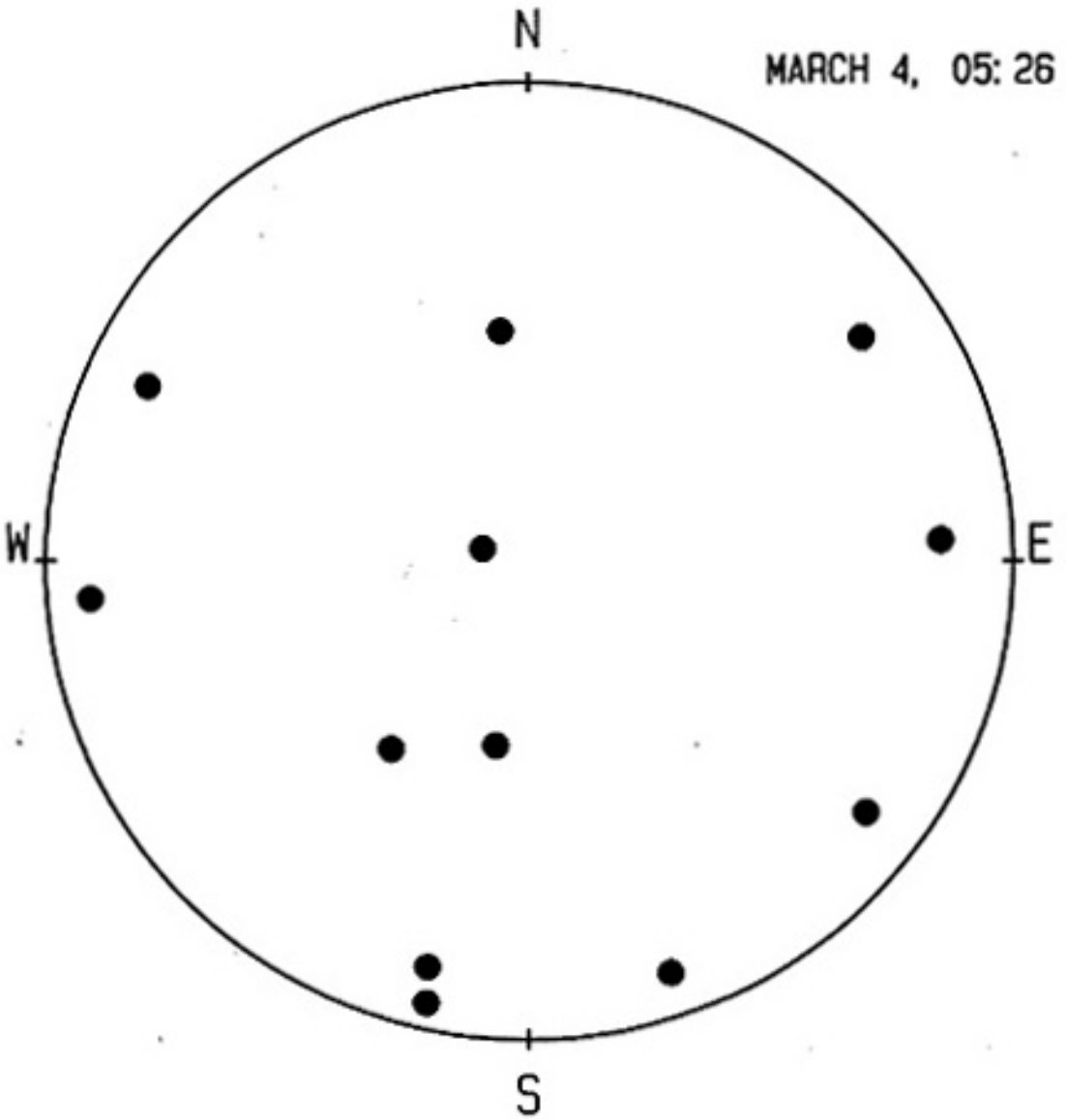

Figure 23. Upper stereographic projection of P-wave first for the earthquake of March 4, 05:26.

intrusion processes may be able to explain the observations. Three possibilities are (1) a double dipole, or linear vector dipole (LVD), (2) a compensated linear vector dipole, and (3) an explosive source. The LVD mechanism is the result of the formation of a tensile crack; the P-wave first motions produced are all compressions (see White, 1965, chapter 5). The CLVD mechanism is similar to the LVD, except that a component is added to provide for the injection of fluid into the crack (see Julian, 1983); the P-wave first motions appear as two 90 degree circles of compression on opposite sides of the focal sphere, with dilatations in between. The third mechanism, an explosive source, may result from the sudden contact of molten rock with water; the P-wave first motions for this source are all compressions.

Both the LVD and the explosive source can explain the two all-compression first motion distributions, but alone they do not satisfy the eleven others. The CLVD mechanism alone cannot explain any of the thirteen unusual first motion diagrams.

Each of the above three fault mechanisms is a mathematical representation of a certain physical process; none of these mathematical models is likely to be an exact representation of the true physical situation. In fact, none of the three models is even a fair representation of the physical situation because none of them can fit all of

the observations. This means that another model is required. One possibility is that the earthquake mechanism is a combination of one or more of the injection mechanisms and a shear dislocation (double couple). At this point there is no way to test this hypothesis because of the extreme non-uniqueness of such a combination of source mechanisms.

CONCLUSIONS

Because previous earthquake swarms in the central Rio Grande rift have been attributed to the movement of molten material into the upper crust, the same mechanism was postulated for the occurrence of the Rest Stop Swarm. The unusual first motion distributions that may be a result of magma injection processes make up the most compelling new evidence from this study in favor of this hypothesis.

If magma migration is indeed the cause of the swarm, then it appears that at least two factors are controlling the path of the upward ascent of the magma from its source, the mid-crustal magma body. They are 1) the local stress field induced by inflation of the mid-crustal magma body, and 2) pre-existing fault zones.

The shallow depth (< 5 km) of some of the RSS earthquakes suggests that magma intrusion in the area may have reached higher levels in the crust than in other areas of the central Rio Grande rift where similar activity is thought to be occurring.

REFERENCES

Ake, J. P., 1984, An analysis of the May and July, 1983 Socorro mountain microearthquake swarms: New Mexico Institute of Mining and Technology, Geophysics Open File Report 49, 107 p.

Ake, J. P., Sanford, A. R., and Jarpe, S. P., 1983, A magnitude scale for central New Mexico based on signal duration: New Mexico Institute of Mining and Technology, Geophysics Open File Report 45, 29 p.

Bachman, G. O., and Mehnert, H. H., 1978, New K-Ar dates and the late Pleistocene to Holocene geomorphic history of the central Rio Grande region, New Mexico: Geological Society of America Bull. 89, 283-292.

Chen, W. P., and Molnar, P., 1983, Focal depths of intracontinental and intraplate earthquakes and their implications for the thermal and mechanical properties of the lithosphere: Journal of Geophysical Research, vol. 88, p. 4183-4214.

Hawley, J. W., ed., 1978, Guidebook to the Rio Grande rift in New Mexico and Colorado: New Mexico Bureau of Mines and Mineral Resources Circular 123.

Julian, B. R., 1983, Evidence for dyke intrusion earthquake mechanisms near Long Valley caldera, California: Nature, vol. 303, p. 323-325.

Larsen, S., and Reilinger, R., 1983, Recent measurements of crustal deformation related to the Socorro magma body, New Mexico, in Chapin, C. E., ed., New Mexico Geological

Society field conference guidebook 34: p. 119-121.

Lee, W. H. K., and Lahr, J. C., 1975, HYPO71 (Revised): A computer program for determining hypocenter, magnitude, and first motion pattern of local earthquakes: U.S. Geological Survey Open-file Report 75-311, 113 p.

Machette, M. N., and McGimsey, R. G., 1983, Quaternary and Pliocene faults in the Socorro and western part of the Fort Sumner 1 x 2 degree quadrangles, New Mexico: U.S. Geological Survey Miscellaneous Field Studies Map MF-1465-A, Pamphlet, 11 p.

Newton, C. A., Cash, D. J., Olsen, K. H., and others, 1976, LASL seismic programs in the vicinity of Los Alamos, New Mexico: Los Alamos Scientific Laboratory Informal Report LA-6046-MS, 42 p.

Reilinger, R. E., Oliver, J. E., Brown, L. D., and others, 1980, New measurements of crustal doming over the Socorro magma body, New Mexico: Geology, vol. 8, p. 291-295.

Reiter, M., Edwards, C. L., Hartman, J., and Wiedman, C., 1975, Terrestrial heat flow along the Rio Grande rift, New Mexico and southern Colorado: Geological Society of Americal Bull. 86, p. 811-818.

Richter, C. F., 1958, Elementary Seismology: W.H. Freeman and Co., San Francisco, 768 p.

Riecker, R. E., ed., 1979, Rio Grande Rift: Tectonics and Magmatism, American Geophysical Union, Washington D. C., 438 p.

Rinehart, E. J., 1979, The determination of an upper crustal model for the Rio Grande rift near Socorro, New Mexico em-

ploying S-wave reflections produced by local microearthquakes: Ph.D. Dissertation, New Mexico Institute of Mining and Technology, Socorro, NM, 92 p.

Rinehart, E. J., Sanford, A. R., and Ward, R. M., 1979, Geographic extent and shape of an extensive magma body at midcrustal depths in the Rio Grande rift near Socorro, New Mexico, in Riecker, R. E., ed., Rio Grande rift: Tectonics and magmatism: American Geophysical Union, Washington, D. C., p. 237-251.

Sanford, A. R., Olsen, K. H., and Jaksha, L. H., 1979, Seismicity of the Rio Grande rift, in Riecker, R. E., ed., Rio Grande rift: Tectonics and magmatism: American Geophysical Union, Washington D. C., p. 145-168.

Sanford, A. R., 1983, Magma bodies in the Rio Grande rift in central New Mexico, in Chapin, C. E., ed., New Mexico Geological Society field conference guidebook 34, p. 123-125.

Sanford, A. R., Jaksha, L. H., ad Wieder, D. P., 1983, Seismicity of the Socorro area of the Rio Grande rift, in Chapin, C. E., ed., New Mexico Geological Society Field Conference Guidebook 34: p. 127-131.

Ward, R. M., 1980, Determination of three-dimensional velocity anomalies within the upper crust in the vicinity of Socorro, New Mexico using P-arrival times from local earthquakes: Ph.D. Dissertation, New Mexico Institute of Mining and Technology, Socorro, NM, 136 p.

Ward, R. M., Schlue, J. W., and Sanford, A. R., 1981, Three dimensional velocity anomalies in the upper crust near

Socorro, New Mexico: Geophysical Research Letters, vol. 8, p. 553-556.

White, J. E., 1965, Seismic Waves: Radiation, Transmission, and Attenuation: McGraw-Hill, 302 p.

Wieder, D. P., 1981, Tectonic significance of microearthquake activity from composite fault-plane solutions in the Rio Grande rift near Socorro, New Mexico: New Mexico Institute of Mining and Technology, Geophysics Open-file Report 37, 159 p.

Appendix 1

Response curves for a typical permanent seismograph station of the NMT-USGS Socorro array and a MEQ-800 seismograph with an L4-C seismometer.

Response Curve For Station BAR

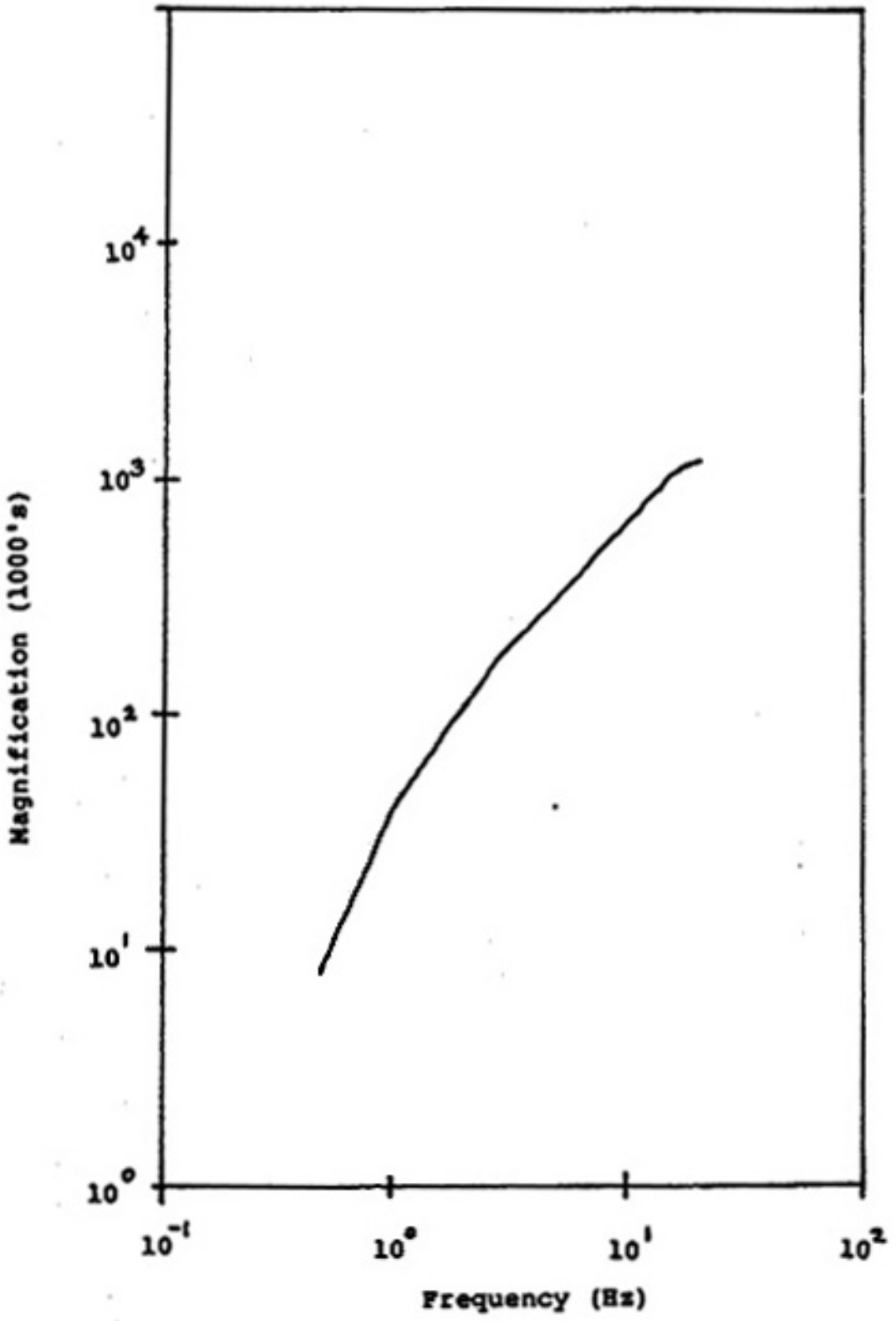

Base Attenuator Setting=12 db

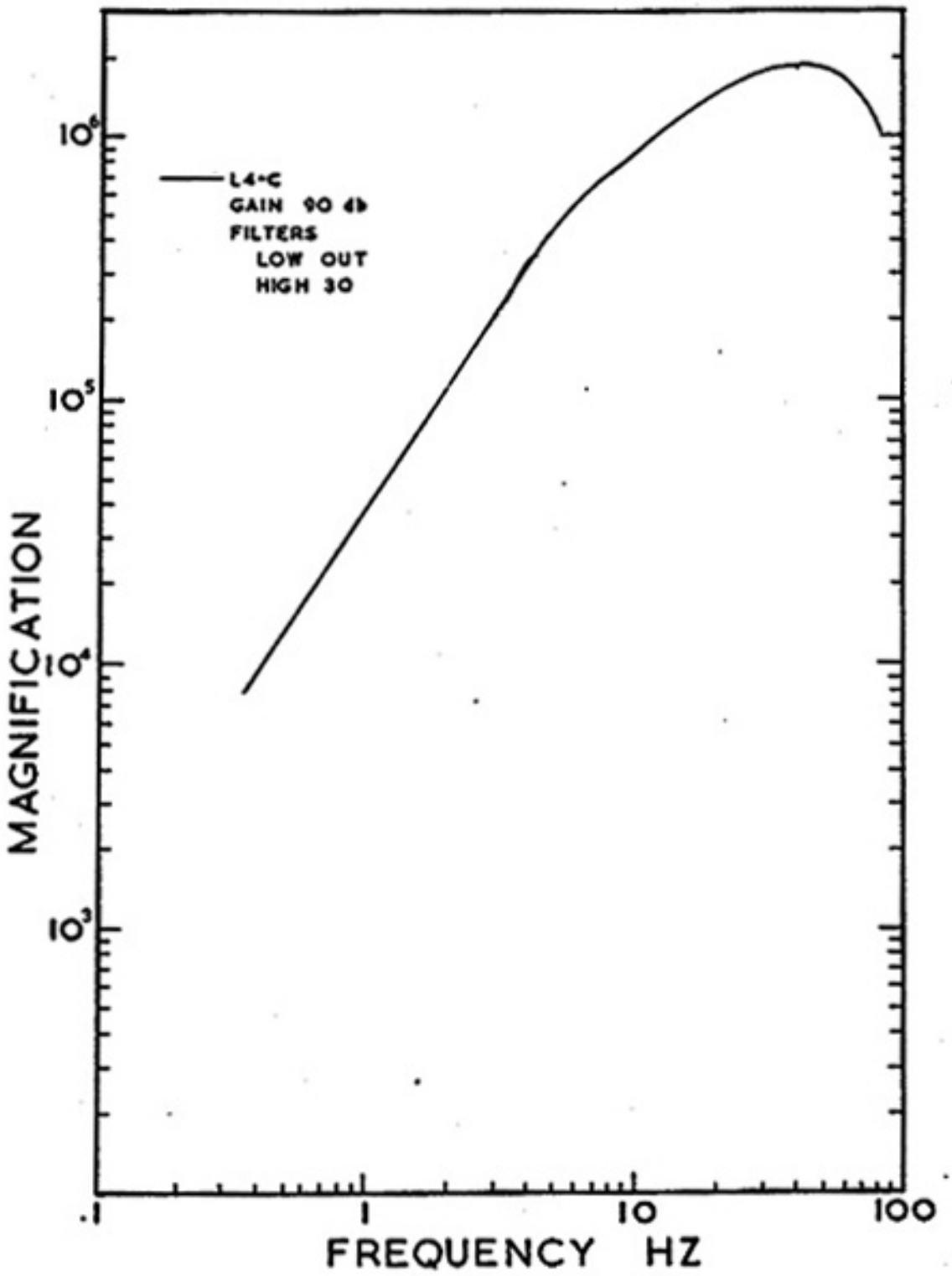

Frequency response of the MEQ-800 with an L4-C seismometer.

Appendix 2

A) A typical HYPO71 output sheet for one of the Rest Stop Swarm locations.

B) Selected HYPO71 output parameters for 60 fixed-depth locations (Table 1.)

C) Selected HYPO71 output parameters for 28 variable-depth locations (Table 2).

DATE AND TIME OF RUN: 4-23-84

03/ 3/ 4 1:47

RESET TO | TEST(1) | TEST(2) | TEST(3) | TEST(4) | TEST(5) | TEST(6) | TEST(7) | TEST(8) | TEST(9) | TEST(10) | TEST(11) | TEST(12) | TEST(13)
0.1000 | 10.0000 | 2.0000 | 0.3500 | 7.0000 | 4.0000 | -3.5300 | 2.7500 | 0.0040 | 100.0000 | 0.0000 | 0.3000 | 5.0000

VELOCITY | DEPTH | ZTR | XMEAN | XFAR | RDS | IU | KNS | KFN | IPUN | IMAG | IK | IPRN | CODE
5.850 | .000 | 7. | 20. | 70. | 1.7320508 | 3 | 1 | 0 | 0 | 1 | 0 | 1 | 1011

												ADJUSTMENTS (KM)			PARTIAL F-VALUES			STANDARD ERRORS			ADJUSTMENTS TAKEN		
I	ORIG	LAT N	LONG W	DEPTH	CK	RMS	AVRPS	SAD	CV	DLAT	DLON	DZ	DLAT	DLON	DZ	DLAT	DLON	DZ	DLAT	DLON	DZ
1	58.33	34-18.32	106-32.36	0.50	0	0.18	0.00	ADJ	2.00	-0.84	-1.38	-1.40	10.91	40.10	9.72	0.20	0.35	0.42	-0.84	-1.38	-1.40
2	58.00	34-17.84	106-32.30	5.00	2	0.07	-0.03	AIA	0.50	0.00	0.00	-0.30	0.04	-1.00	0.56	0.00	0.00	0.40	0.00	0.00	-0.30
3	58.50	34-17.84	106-32.30	4.80	2	0.07	0.00	AIA	0.50	0.05	0.00	0.00	0.05	-1.00	-1.00	0.21	0.00	0.00	0.00	0.00	0.00
4	58.50	34-17.84	106-32.30	4.80	2	0.07	0.00	AZA	2.00	0.05	0.01	0.00	0.04	0.00	0.00	0.24	0.24	0.49	0.00	0.00	0.00

DATE	ORIGIN	LAT N	LONG W	DEPTH	MAG	NO	DM	GAP	M	RMS	ERH	ERZ	Q	SOD	ADJ	IN	AR	ATR	AAR	NM	ATXM	SDXM	AF	AYFM	SDYM	I
830304	1 17 58.50	34-17.84	106-32.30	4.80	1.87	12	2	66	1	0.07	0.3	0.5	A	AIA	0.30	10	13	0.00	0.05	0	0.0	0.0	3	1.9	0.0	3

STN	DIST	AZM	AIN	PHASE	ARRS	P-SEC	TRES	TCAL	DLY/MI	P-WTS	P-WTI	AMX	PMX	CALX	K	XMAG	RMK	FNP	FMAG	SRMK	S-SEC	TSRES	S-WES	S-WT	DT
NSV	1.6	295	162	P	0	147	57.94	0.58	0.86	-0.25	-0.01	1.44	0	0	0.00	0									
BAD	4.0	194	148	P	0	147	57.50	1.00	1.07	-0.10	0.02	1.19	0	0	0.00	0									
ALA	5.6	223	130	P	0	147	57.35	1.45	1.26	0.14	0.05	1.49	0	0	0.00	0									
SLV	9.2	348	108	P	0	147	57.95	1.40	1.24	0.11	-0.00	1.39	0	0	0.00	0									
BMN	12.1	358	108	P	0	146	0.35	1.85	1.77	0.13	0.02	1.48	0	0	0.00	0									
LVK	21.1	165	102	P	0	148	0.33	2.50	4.04	-0.06	0.02	1.07	0	0	0.00	0									
RTA	23.0	195	102	P	0	148	0.33	2.35	4.26	-0.06	-0.04	1.11	0	0	0.00	0			S	3	5.60	9.30	1.58**	.40	
FAR	24.3	205	102	P	0	148	0.33	2.35	4.32	-0.06	-0.04	1.03	0	0	0.00	0		95	1.47						
BRK	24.3	147	100	P	0	148	0.35	4.85	4.31	0.00	-0.05	1.23	0	0	0.00	0		90	1.8						
CHN	25.7	188	98	P	2	148	0.35	2.15	4.51	0.01	-0.04	1.31	0	0	0.00	0									
MC	30.1	193	95	P	2	148	0.35	10.15	10.14	0.05	-0.03	1.10	0	0	0.00	0		95	1.9						

LAT	LON	Z	AVRPS	RMS			DRMS		
20.34	55.38	0.00	-0.14	0.65		0.59			
20.34	49.04	0.00	-0.15	0.76		(0.51)		0.64	
20.34	55.38	9.80	-0.28	0.58				(0.69)	
20.34	49.04	9.80	-0.69	0.76					
17.84	52.30	0.00	0.23	0.19			0.12		
				0.07			0.00		
17.84	52.30	13.46	-0.86	0.43			(0.37)		
15.34	55.38	0.00	0.02	0.74		0.67			
15.34	49.04	0.00	-0.01	0.74				0.67	
15.34	55.38	9.80	-0.33	0.88		(0.59)		(0.79)	
15.34	49.04	9.80	-0.33	0.88					

Table 1. HYPO71 Output Parameters for the 60 Fixed-Depth Solutions.

Date	Origin time (hr,min,sec)	Location Lat-N (deg-min)	Location Long-W (deg-min)	Depth (km)	M_L	Gap (deg)	RMS (sec)	Erh (km)	Erz (km)	Q
830225	257 54.51	34-18.54	106-52.07	6.50*	2.19	113	0.07	0.5	3.5	C
830225	849 55.05	34-18.75	106-52.10	6.50*	1.34	155	0.08	0.6	2.9	C
830226	1115 41.29	34-18.35	106-52.20	6.50*	2.53	112	0.11	0.5	4.5	C
830226	1120 55.86	34-19.78	106-51.73	6.50*	0.55	168	0.19	2.6	10.3	C
830226	1136 43.99	34-19.61	106-51.46	6.50*	0.66	166	0.23	1.1	7.0	C
830226	1554 37.50	34-19.80	106-51.68	6.50*	0.56	168	0.23	1.1	5.6	C
830226	1719 43.15	34-18.87	106-52.17	6.50*	0.59	159	0.08	0.6	3.4	C
830226	19 0 42.40	34-19.55	106-51.92	6.50*	0.93	165	0.13	0.6	3.7	C
830226	2223 22.97	34-18.87	106-51.93	6.50*	0.47	159	0.09	0.5	2.9	C
830228	12 4 39.93	34-18.55	106-51.98	6.50*	0.54	157	0.18	0.8	4.2	C
830228	1349 13.12	34-17.93	106-52.06	6.50*	1.33	151	0.09	0.3	2.0	B
830228	2312 41.94	34-18.36	106-52.36	6.50*	1.92	112	0.07	0.3	1.9	B
830302	18 5 46.08	34-18.85	106-52.05	6.50*	1.21	115	0.09	0.4	3.3	C
830302	1814 33.27	34-18.87	106-52.11	6.50*	1.02	159	0.08	0.4	3.1	C
830302	2322 19.43	34-17.99	106-52.74	6.50*	4.00	109	0.10	0.7	6.2	C

Date	Origin time (hr,min,sec)	Location Lat-N (deg-min)	Location Long-W (deg-min)	Depth (km)	M_L	Gap (deg)	RMS (sec)	Erh (km)	Erz (km)	Q
830302	2344 9.11	34-18.45	106-52.27	6.50*	0.39	155	0.07	0.3	1.8	B
830302	2348 15.66	34-18.47	106-52.14	6.50*	1.22	113	0.12	0.5	4.2	C
830302	2349 45.51	34-17.57	106-53.04	6.50*	0.82	188	0.10	0.4	2.0	C
830302	2350 36.21	34-18.41	106-52.39	6.50*	2.50	153	0.04	0.4	3.2	C
830303	032 39.00	34-19.20	106-52.34	6.50*	1.37	162	0.09	1.0	10.0	C
830303	047 50.46	34-18.00	106-52.38	6.50*	0.47	152	0.06	0.6	6.0	C
830303	118 38.34	34-18.65	106-51.94	6.50*	0.50	158	0.20	0.6	4.1	C
830303	2 6 27.87	34-18.36	106-52.19	6.50*	1.64	112	0.04	0.3	3.1	C
830303	222 15.38	34-20.45	106-51.35	6.50*	0.60	174	0.21	1.6	9.1	C
830303	3 4 59.38	34-18.24	106-52.40	6.50*	0.78	153	0.06	5.0	45.4	C
830303	429 34.50	34-18.46	106-52.50	6.50*	1.26	155	0.04	0.3	3.3	C
830303	631 59.16	34-17.96	106-52.46	6.50*	1.15	151	0.08	0.8	8.2	C
830303	8 5 11.82	34-18.52	106-52.04	6.50*	1.24	156	0.04	4.1	35.3	C
830303	910 12.40	34-17.97	106-52.40	6.50*	0.83	151	0.04	3.6	34.4	C
830303	923 48.76	34-18.96	106-52.51	6.50*	1.22	159	0.13	2.3	22.0	C

Date	Origin time (hr,min,sec)	Location Lat-N (deg-min)	Location Long-W (deg-min)	Depth (km)	M_L	Gap (deg)	RMS (sec)	Erh (km)	Erz (km)	Q
830303	1119 12.65	34-18.22	106-51.98	6.50*	1.67	112	0.08	0.5	5.4	C
830303	1133 51.43	34-18.51	106-51.60	6.50*	0.56	157	0.09	0.9	8.4	C
830303	16 7 14.83	34-18.03	106-51.78	6.50*	1.00	152	0.02	0.2	2.6	C
830303	1740 11.51	34-18.56	106-51.87	6.50*	1.92	114	0.06	0.3	2.7	C
830303	2235 28.23	34-17.75	106-52.58	6.50*	1.02	149	0.05	0.4	3.4	C
830304	0 0 22.02	34-18.02	106-52.64	6.50*	1.99	110	0.09	0.2	1.9	B
830304	147 56.45	34-17.74	106-52.23	6.50*	1.87	149	0.09	0.6	6.4	C
830304	149 24.26	34-18.04	106-52.46	6.50*	1.30	152	0.03	0.1	1.1	B
830304	326 49.33	34-18.53	106-52.41	6.50*	0.73	156	0.08	0.3	1.9	B
830304	526 10.46	34-18.28	106-52.54	6.50*	1.90	154	0.06	0.4	4.4	C
830304	1820 6.70	34-18.66	106-52.04	6.50*	1.10	158	0.16	0.8	7.7	C
830304	2149 21.20	34-19.20	106-52.29	6.50*	0.84	162	0.10	0.8	7.6	C
830305	11 5 25.39	34-18.15	106-51.37	6.50*	0.93	154	0.11	0.6	5.3	C
830306	011 21.68	34-18.14	106-51.94	6.50*	0.96	153	0.05	0.5	5.0	C
830306	3 0 50.84	34-17.72	106-51.86	6.50*	0.51	150	0.06	0.5	5.6	C

Date	Origin time (hr,min,sec)	Location Lat-N (deg-min)	Location Long-W (deg-min)	Depth (km)	M_L	Gap (deg)	RMS (sec)	Erh (km)	Erz (km)	Q
830306	2213 29.64	34-17.56	106-52.92	6.50*	0.91	147	0.08	2.1	20.7	C
830306	2326 23.02	34-17.84	106-52.19	6.50*	0.60	150	0.04	0.4	4.0	C
830308	6 6 44.74	34-18.34	106-52.78	6.50*	1.24	94	0.05	0.3	0.4	B
830308	619 0.02	34-18.40	106-52.64	6.50*	2.03	112	0.06	0.4	4.0	C
830308	827 29.10	34-17.61	106-51.72	6.50*	1.42	149	0.04	0.3	2.7	C
830308	16 4 43.07	34-18.88	106-51.63	6.50*	0.90	160	0.07	0.8	7.4	C
830309	9 5 59.03	34-18.46	106-52.57	6.50*	1.69	112	0.06	0.4	4.0	C
830309	15 3 24.90	34-18.31	106-52.53	6.50*	0.84	154	0.06	0.5	5.4	C
830309	23 3 25.96	34-18.63	106-52.56	6.50*	0.72	157	0.03	0.2	2.3	C
830309	2325 34.86	34-18.12	106-52.60	6.50*	1.24	152	0.06	0.6	6.0	C
830311	11 7 1.35	34-17.93	106-51.93	6.50*	0.63	151	0.15	1.2	9.2	C
830312	21 8 16.22	34-18.47	106-52.09	6.50*	0.90	156	0.07	0.5	4.4	C
830315	927 2.80	34-17.42	106-52.50	6.50*	2.12	107	0.06	0.4	4.6	C
830316	830 29.00	34-17.65	106-52.39	6.50*	1.15	149	0.08	0.8	8.7	C
830317	2235 52.43	34-18.03	106-52.94	6.50*	2.89	109	0.03	0.3	2.5	C

Table 2. HYPO71 Output Parameters for the 28 High-Quality Solutions.

Date	Origin time (hr,min,sec)	Location Lat-N (deg-min)	Location Long-W (deg-min)	Depth (km)	M_L	Gap (deg)	RMS (sec)	Erh (km)	Erz (km)	Q
830303	2 6 27.84	34-18.26	106-52.18	7.42	1.64	112	0.05	0.3	0.6	B
830303	1119 12.63	34-18.15	106-51.97	7.25	1.67	111	0.08	0.5	0.6	B
830303	16 7 14.76	34-18.09	106-51.70	7.89	1.00	108	0.06	0.4	0.5	B
830303	1740 11.47	34-18.47	106-51.95	7.45	1.92	108	0.04	0.3	0.3	B
830303	2235 28.29	34-17.89	106-52.54	4.80	1.02	94	0.06	0.3	0.4	B
830304	0 0 22.04	34-18.29	106-52.59	5.72	1.99	66	0.10	0.5	0.7	A
830304	147 56.50	34-17.84	106-52.30	4.80	1.87	66	0.07	0.3	0.5	A
830304	149 24.28	34-18.06	106-52.50	6.77	1.30	66	0.05	0.3	0.3	A
830304	326 49.27	34-18.90	106-52.30	7.86	0.73	76	0.09	0.5	0.7	A
830304	526 10.52	34-18.04	106-52.65	6.50	1.90	64	0.07	0.3	0.4	A
830304	1353 28.70	34-18.48	106-52.73	5.78	0.57	125	0.06	0.4	0.5	B
830304	1820 6.80	34-17.79	106-52.36	4.97	1.10	65	0.13	0.7	0.9	A
830304	2149 21.30	34-18.47	106-52.52	5.88	0.84	68	0.09	0.5	0.7	A
830305	11 5 25.43	34-17.63	106-51.59	5.67	0.93	72	0.06	0.4	0.6	A

Date	Origin time (hr,min,sec)	Location Lat-N (deg-min)	Location Long-W (deg-min)	Depth (km)	M_L	Gap (deg)	RMS (sec)	Erh (km)	Erz (km)	Q
830306	011 21.66	34-18.07	106-52.03	7.40	0.96	72	0.05	0.3	0.5	A
830306	3 0 50.82	34-17.79	106-51.93	7.01	0.51	70	0.05	0.3	0.5	A
830306	2213 29.64	34-17.83	106-52.72	6.50	0.91	91	0.09	0.7	0.8	B
830306	2326 23.00	34-17.98	106-52.16	6.50	0.60	100	0.05	0.4	0.6	B
830308	6 6 44.67	34-18.47	106-52.64	7.32	1.24	97	0.05	0.3	0.5	B
830308	619 0.03	34-18.24	106-52.71	6.40	2.03	94	0.05	0.3	0.4	B
830308	827 29.08	34-17.53	106-51.75	7.28	1.42	101	0.04	0.2	0.4	B
830308	16 4 43.02	34-19.12	106-51.42	7.10	0.90	127	0.07	0.6	0.8	B
830309	9 5 59.11	34-18.08	106-52.71	5.71	1.69	96	0.05	0.3	0.4	B
830309	15 3 24.95	34-18.29	106-52.55	5.88	0.84	98	0.07	0.5	0.7	B
830309	23 3 26.03	34-18.29	106-52.69	5.75	0.72	97	0.07	0.4	0.6	B
830309	2325 34.92	34-18.10	106-52.66	5.60	1.24	96	0.07	0.4	0.6	B
830311	11 7 1.38	34-17.64	106-52.13	5.18	0.63	97	0.08	0.5	0.7	B
830311	1146 13.40	34-18.82	106-51.89	6.50	0.61	109	0.09	0.6	1.0	B

Appendix 3

Upper focal sphere projections of P-wave first motions for 26 Rest Stop Swarm earthquakes.

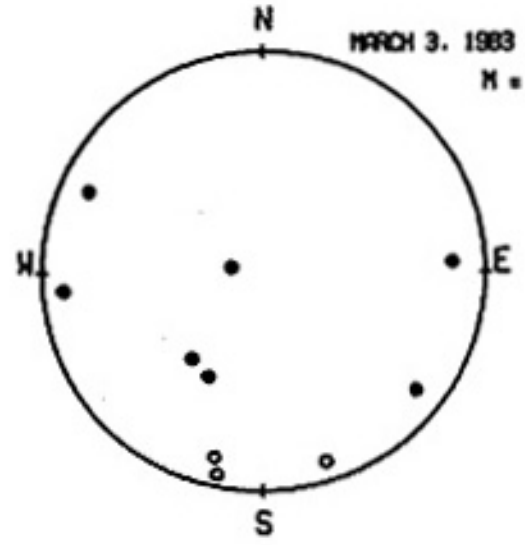
N
MARCH 3. 1983 06:31
M = 1.2
W
E
S

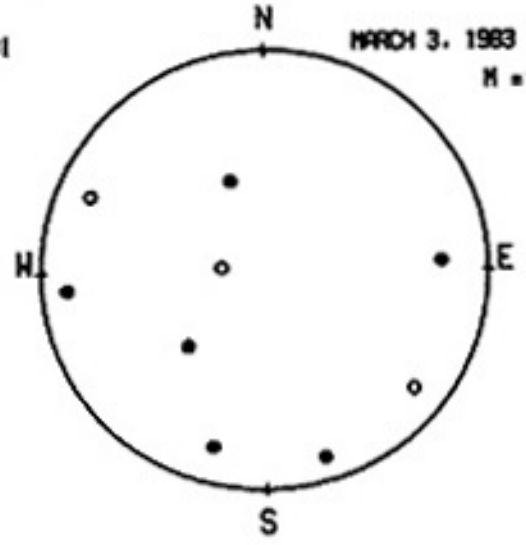
N
MARCH 3. 1983 16:07
M = 1.0
W
E
S

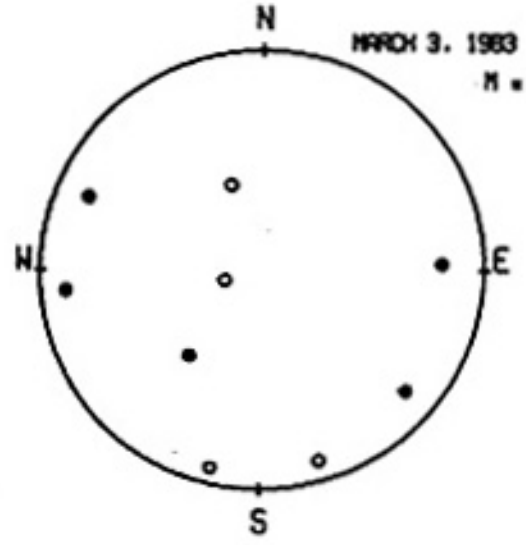
N
MARCH 3. 1983 17:40
M = 1.9
W
E
S

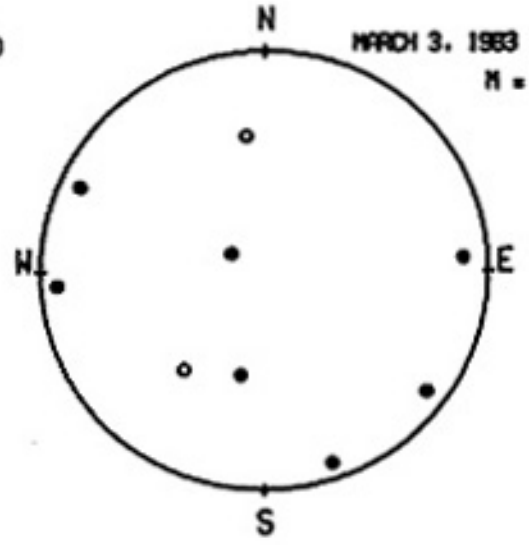
N
MARCH 3. 1983 22:35
M = 1.0
W
E
S

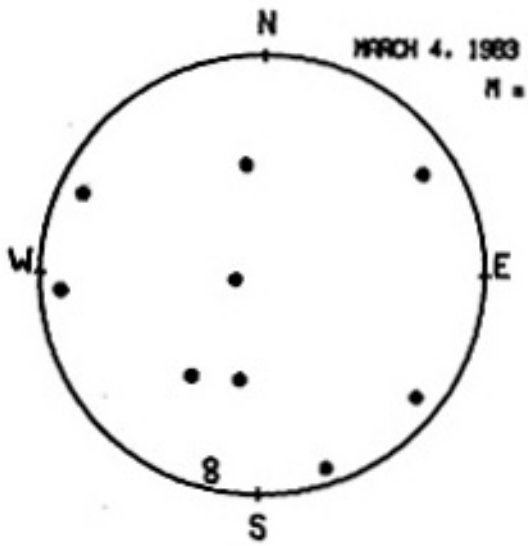
N
MARCH 4. 1983 00:00
M = 2.0
W
E
S

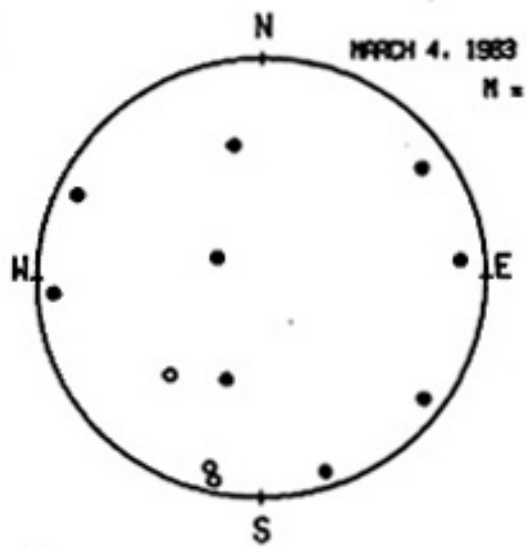
N
MARCH 4. 1983 01:47
M = 1.9
W
E
S

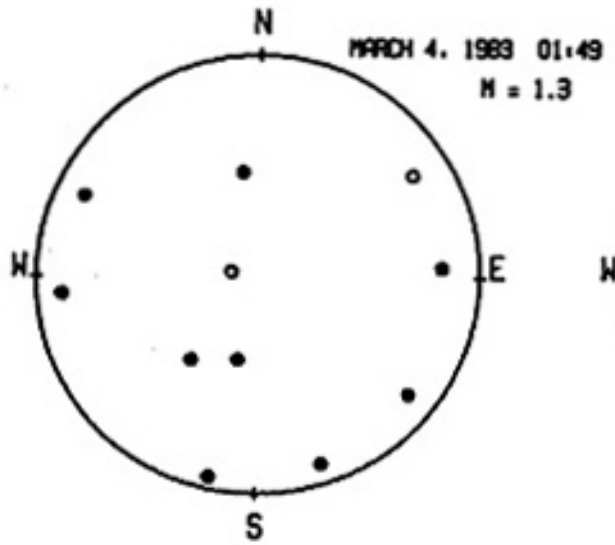
N
MARCH 4. 1983 01:49
M = 1.3
W
E
S

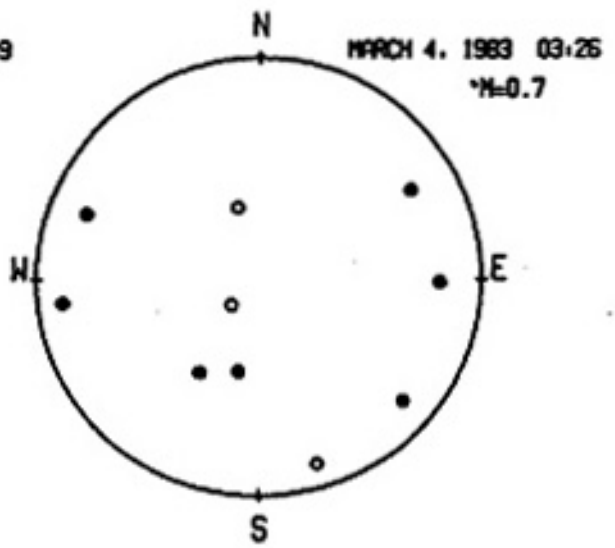
N
MARCH 4. 1983 03:26
M=0.7
W
E
S

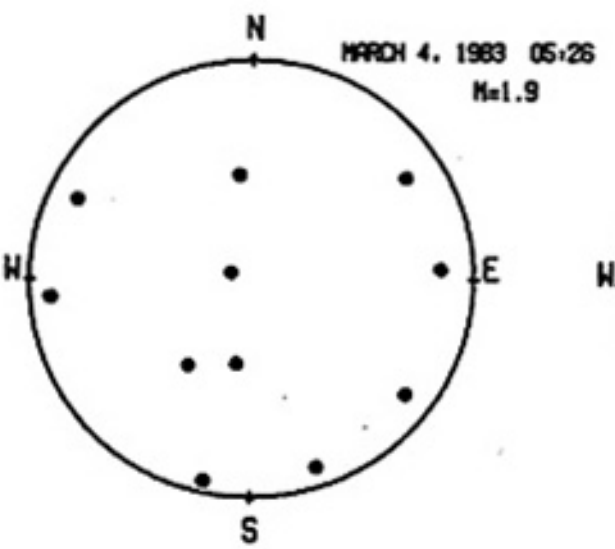
N
MARCH 4. 1983 05:26
M=1.9
W
E
S

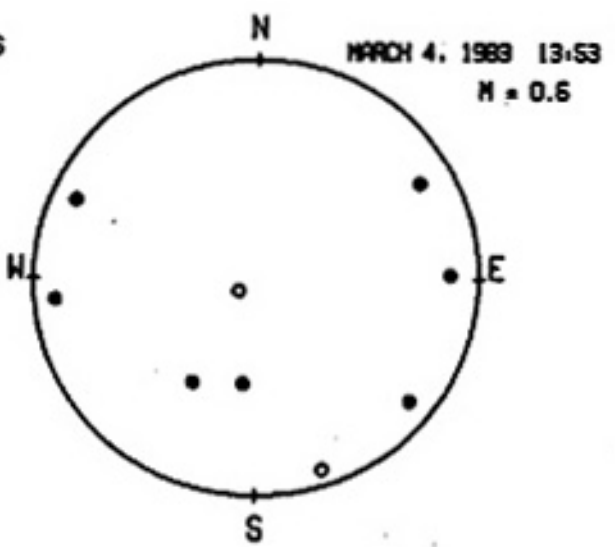
N
MARCH 4. 1983 13:53
M = 0.6
W
E
S

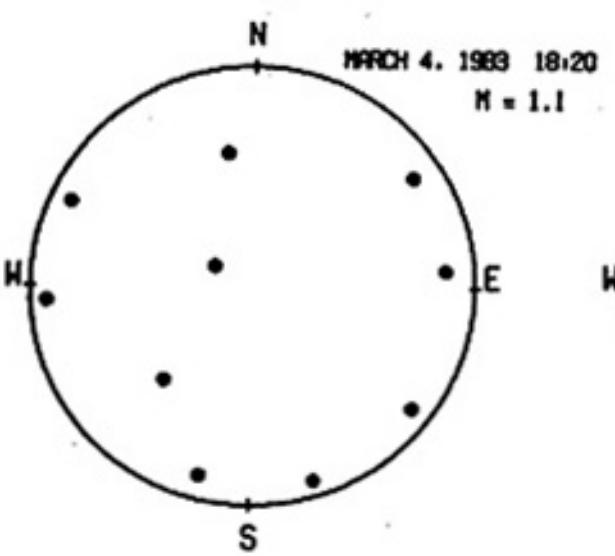
N
MARCH 4. 1983 18:20
M = 1.1
W
E
S

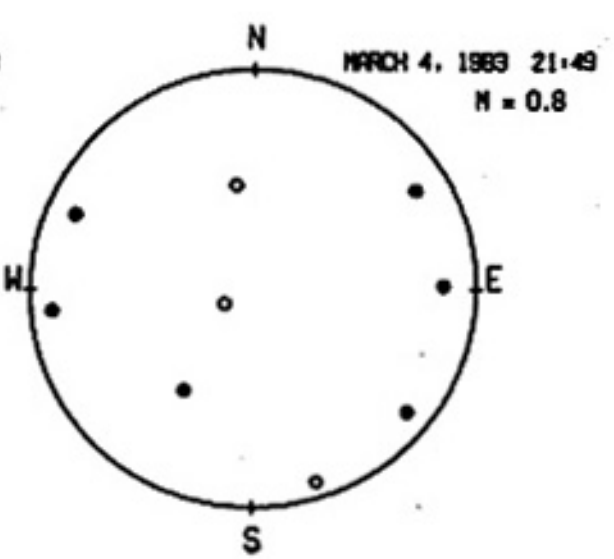
N
MARCH 4. 1983 21:49
M = 0.8
W
E
S

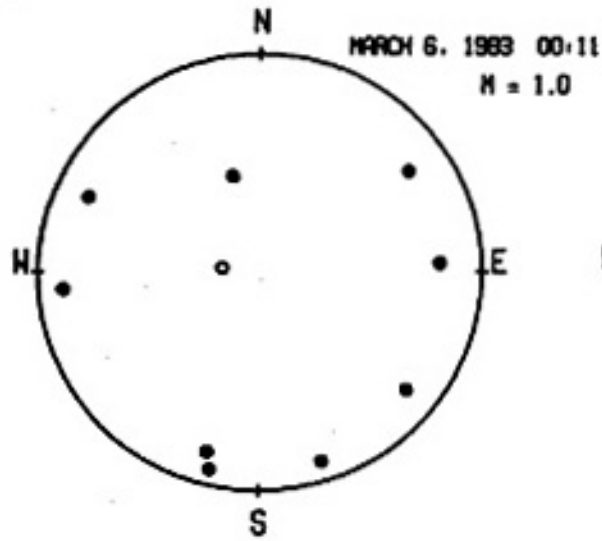
N
MARCH 6. 1983 00:11
M = 1.0
W
E
S

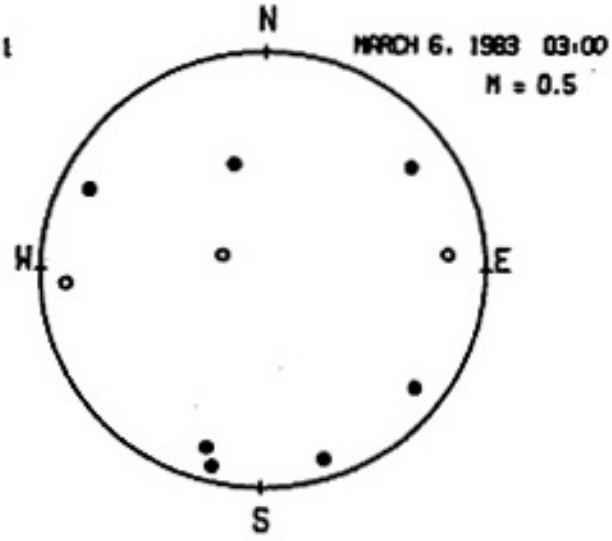
N
MARCH 6. 1983 03:00
M = 0.5
W
E
S

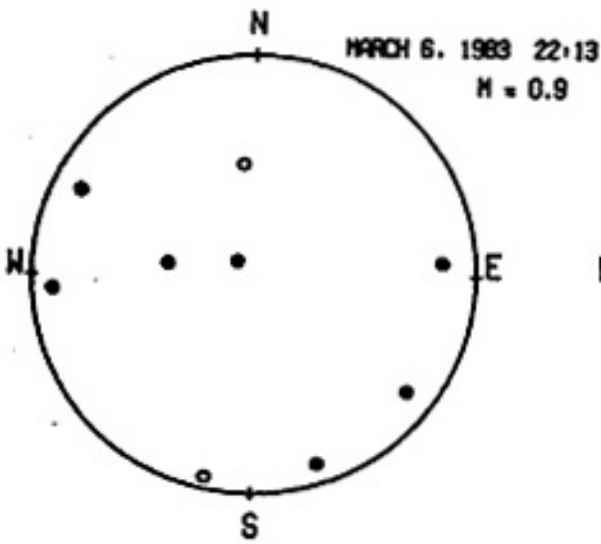
N
MARCH 6. 1983 22:13
M = 0.9
W
E
S

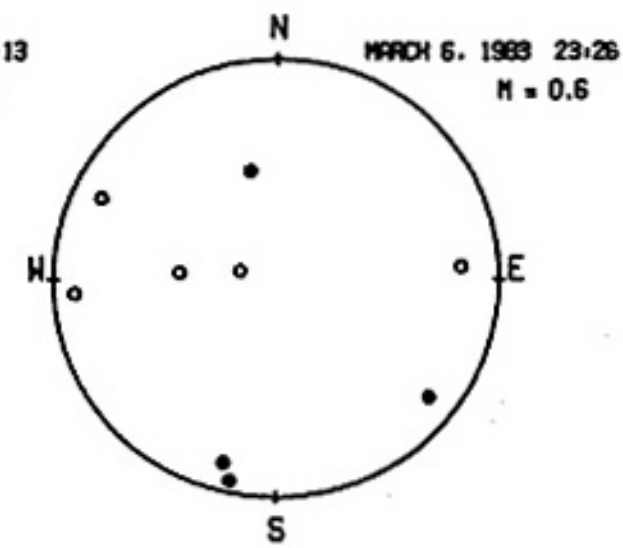
N
MARCH 6. 1983 23:26
M = 0.6
W
E
S

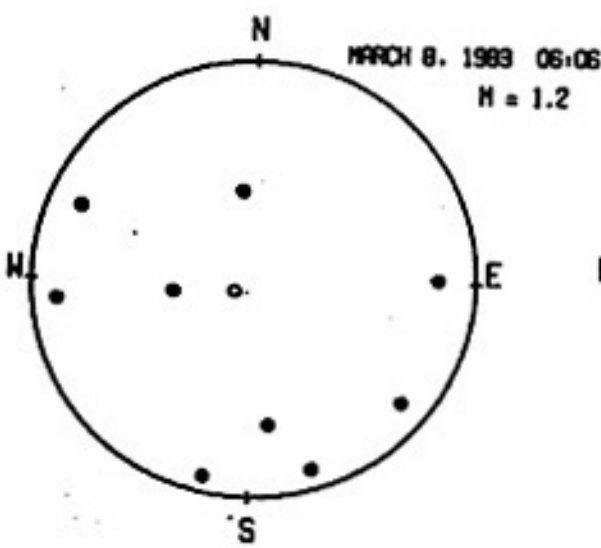
N
MARCH 8. 1983 06:06
M = 1.2
W
E
S

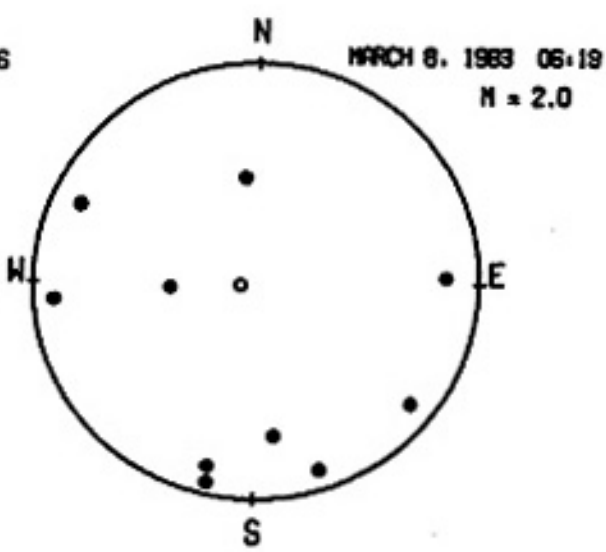
N
MARCH 8. 1983 06:19
M = 2.0
W
E
S

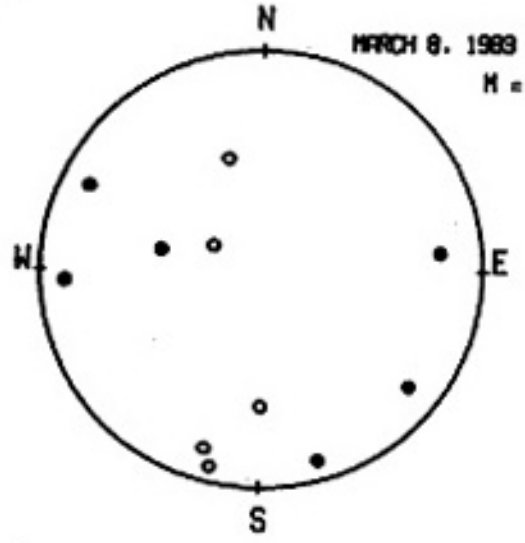
N
MARCH 8. 1983 08:27
M = 1.4
W
E
S

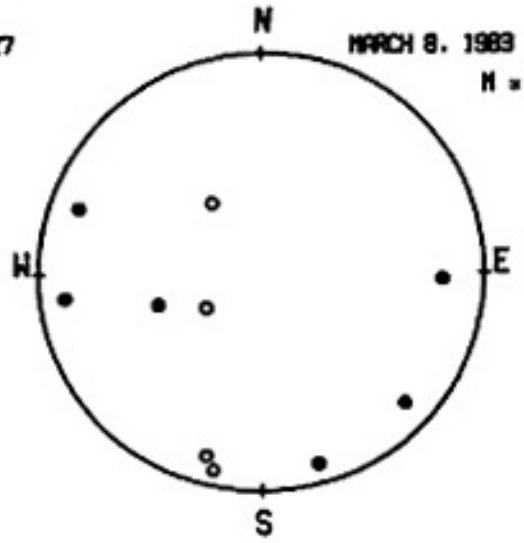
N
MARCH 8. 1983 16:04
M = 0.9
W
E
S

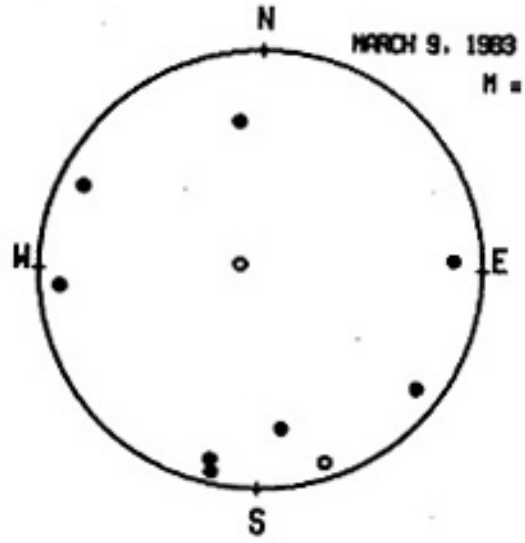
N
MARCH 9. 1983 09:05
M = 1.7
W
E
S

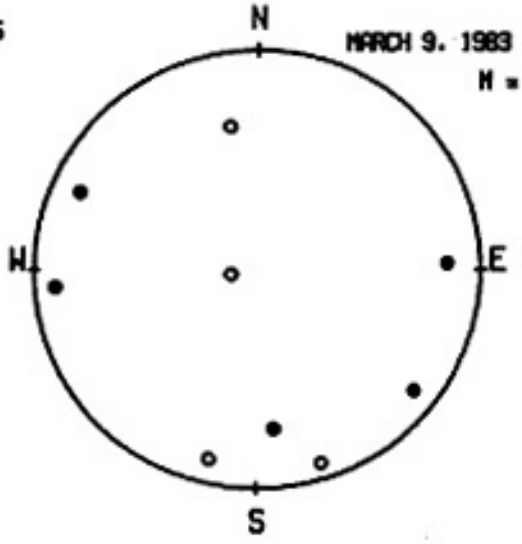
N
MARCH 9. 1983 15:03
M = 0.8
W
E
S

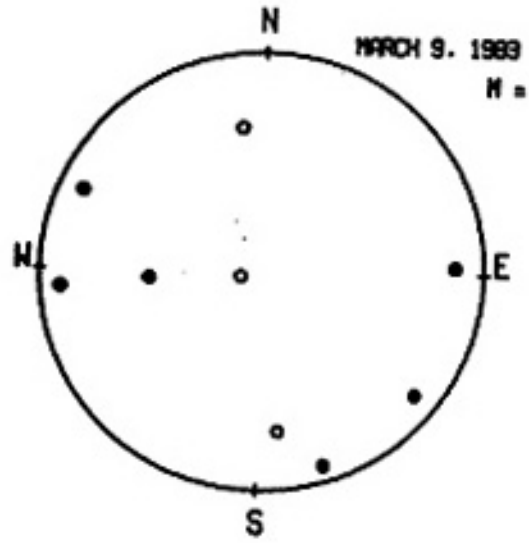
N
MARCH 9. 1983 23:03
M = 0.7
W
E
S

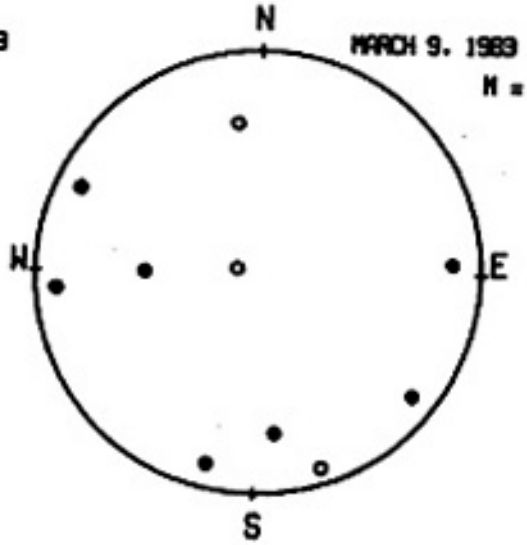
N
MARCH 9. 1983 23:25
M = 1.2
W
E
S

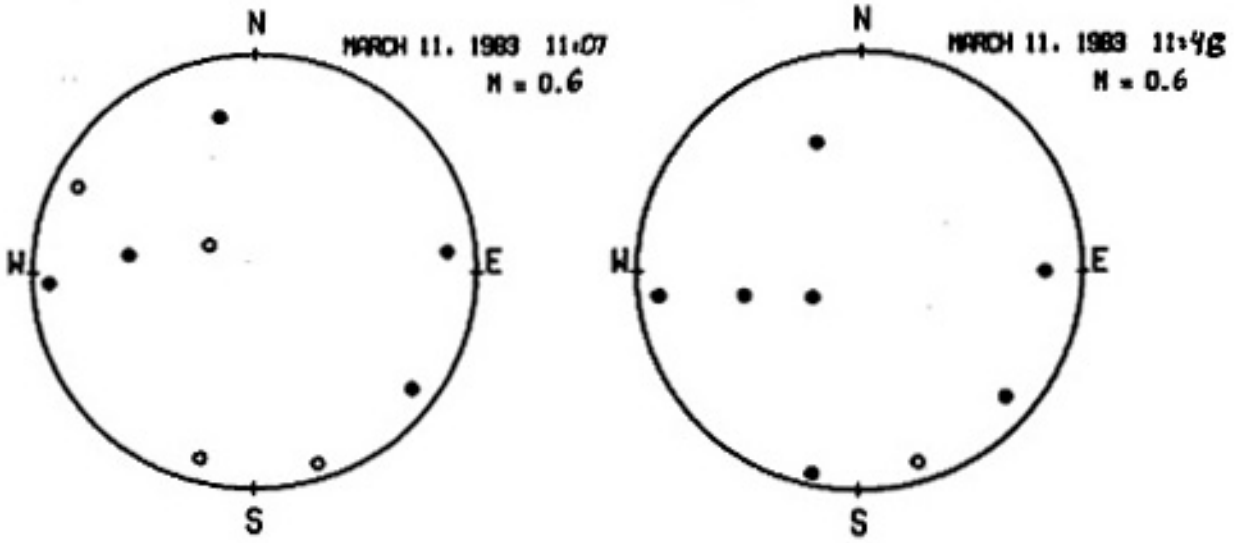
N
MARCH 11. 1983 11:07
M = 0.6
W
E
S
N
MARCH 11. 1983 11:49
M = 0.6
W
E
S

APPENDIX 4

Some measurements of $\tau_{1/2}$ from high-quality analog records (drum speed 120 mm/min) measured with a precision travelling microscope having a resolution of +/- 0.0005 sec. are presented here. Table 1 gives the average $\tau_{1/2}$ for small events presumably below the magnitude at which duplication of $\tau_{1/2}$ ends. Table 2 has measurements of $\tau_{1/2}$ for events having magnitudes near or above the duplication threshold that have had the average for $\tau_{1/2}$ at that station subtracted from them. The quality of the measurements at stations RSD and SAD should be considered the best because the records were on smoked paper.

Table 1. Determination of the Minimum τ_{y_L} for Each of the Five Stations from Measurements of Small Events.

Station	RSD	SAD	ALA	LJ1	BB2
(sec)	0.052	0.061	0.072	0.076	0.104
No. of readings	21	4	17	14	8
Stand. dev.	0.006	0.013	0.013	0.010	0.008

Table 2. Measurements of Residual τ_{y_L} for Some Events with $M_L > 0.5$.

		RSD	SAD	ALA	LJ1	BB2
Event	M_L					
3/3 0923	1.2	0.033		0.003		
3/3 1119	1.7	0.023		0.023		
3/3 1607	1.0	0.013		0.038		
3/3 1740	1.9	0.073			0.054	
3/3 2235	1.0		0.014	0.028	0.039	
3/4 0000	2.0		0.067	0.053	0.089	
3/4 0147	1.8		0.059	0.048	0.024	
3/4 0149	1.4		0.044	0.023	0.034	
3/4 0326	0.7	0.008	0.004	0.028		0.021
3/4 0526	1.9		0.054	0.078	0.014	
3/4 1353	0.6		0.034	0.013		
3/4 1820	1.1	0.084		0.028	0.014	0.051
3/4 2149	0.8	0.032		0.053	0.024	0.004
3/5 1105	0.9	0.048				
3/6 0011	1.0	0.023				
3/6 0300	0.5	0.010				
3/6 2326	0.6	0.008				
3/8 0606	1.2	0.018				
3/8 0619	2.0	0.028				
3/8 1604	0.9	0.017				
3/9 0906	1.7	0.043				
3/9 2325	1.2	0.028				
3/111117	0.6	0.021				
3/111146	0.6	0.013				